Compound Heat Wave, Drought, and Dust Events in California

BING PU,[a] QINJIAN JIN,[a] PAUL GINOUX,[b] AND YAN YU[c]

[a] *Department of Geography and Atmospheric Science, University of Kansas, Lawrence, Kansas*
[b] *NOAA/Geophysical Fluid Dynamics Laboratory, Princeton, New Jersey*
[c] *Department of Atmospheric and Oceanic Sciences, Peking University, Beijing, China*

(Manuscript received 17 November 2021, in final form 23 August 2022)

ABSTRACT: California is one of the nation's top agriculture producers and is vulnerable to extreme events such as droughts and heat waves. Concurrent extreme events may further stress water and energy resources, exerting greater adverse socioeconomic, environmental, and health impacts than individual events. Here we examine the features of compound drought, heat wave, and dust events in California during spring and summer. From 2003 to 2020, 16 compound events are found in warm seasons, with a mean duration of ~4 days. Compound events are characterized by enhanced surface temperature up to 4.5°C over northern and western California, reduced soil moisture and vegetation density, and an increase in dust optical depth (DOD) by 0.05–0.1 over central and southern California. The enhanced DOD is largely associated with severe vegetation dieback that favors dust emissions and southeasterly wind anomalies that support northward transport of dust from source regions in southern California. Surface fine dust and $PM_{2.5}$ concentrations also increase by more than 0.5 and 5 $\mu g\ m^{-3}$, respectively, during compound events associated with both enhanced dust emissions and a relatively stable atmosphere that traps pollutants. The development of the compound events is related to an anomalous high over the west coast in the lower to middle troposphere, which is a pattern favoring sinking motion and dry conditions in California. The anomalous high is embedded in a wave train that develops up to 7 days before the events. In comparison with heat wave extremes alone, compound events show significantly higher DOD and lower vegetation density associated with droughts.

KEYWORDS: North America; Drought; Dust or dust storms; Extreme events; Air pollution

1. Introduction

California produces about one-half of all fresh fruits and vegetables consumed by Americans and supplies about 15% of U.S. agricultural exports (Christian-Smith et al. 2011). Extreme events, such as droughts and heat waves, have far-reaching socioeconomic and environmental impacts. Two recent severe droughts during 2007–09 and 2011–16 (Seager et al. 2015; Xiao et al. 2017; Ullrich et al. 2018) cost more than $6 billion through agriculture loss and a large reduction in hydropower production due to low runoff and water storage (Christian-Smith et al. 2011; Lund et al. 2018).

While most studies focus on the mechanisms and impacts of individual extreme events, simultaneously occurring climate extremes, referred to as compound events, have recently come to attention. Extremely high temperatures accompanied the 2011–16 California drought (e.g., Seager and Hoerling 2014), and heat waves were reported in June 2008, 2013, and 2016 in central and southern California (e.g., Lee and Grotjahn 2016). The co-occurrence of extreme events may intensify the impacts of individual events, further stressing energy and water resources and having adverse impacts on environment and human health. Severe droughts can increase dust emissions over the southwestern United States (Pu and Ginoux 2017), where dust is an important component of the total particulate matter below 2.5 μm ($PM_{2.5}$) mass in spring and summer (Hand et al. 2017) and can influence the strength of North American monsoon (Zhao et al. 2012). Such a coexistence of droughts and enhanced dustiness is also evident in California in the recent decade (Fig. 1).

Substantial increases in concurrent droughts and heat waves are found over large parts of the United States since 1960 (Mazdiyasni and AghaKouchak 2015). Climate models have projected unprecedented drying conditions over the southwestern United States in the late twenty-first century (e.g., Seager and Vecchi 2010; Cook et al. 2015) and increases in heat waves due to increasing greenhouse gas concentrations (Gershunov and Guirguis 2012; Palipane and Grotjahn 2018). While future variations in dust emissions still have large uncertainties, projections with observational constraints suggest an increase in dustiness in southern California during the dry season in association with climate change (Pu and Ginoux 2017, 2018b). Understanding compound extreme events in the present will help project their future impacts as they likely become more frequent.

In this paper, we focus on concurrent drought, heat wave, and dust events in California. We will examine the occurrence, characteristics, formation, and air quality impacts of the compound events using satellite products, ground observations, and reanalyses from 2003 to 2020. The method developed here may be applied to other regions to understand compound events.

Denotes content that is immediately available upon publication as open access.

Supplemental information related to this paper is available at the Journals Online website: https://doi.org/10.1175/JCLI-D-21-0889.s1.

Corresponding author: Bing Pu, bpu@ku.edu

DOI: 10.1175/JCLI-D-21-0889.1

© 2022 American Meteorological Society. For information regarding reuse of this content and general copyright information, consult the AMS Copyright Policy (www.ametsoc.org/PUBSReuseLicenses).

Brought to you by NOAA Central Library | Unauthenticated | Downloaded 07/19/23 05:08 PM UTC

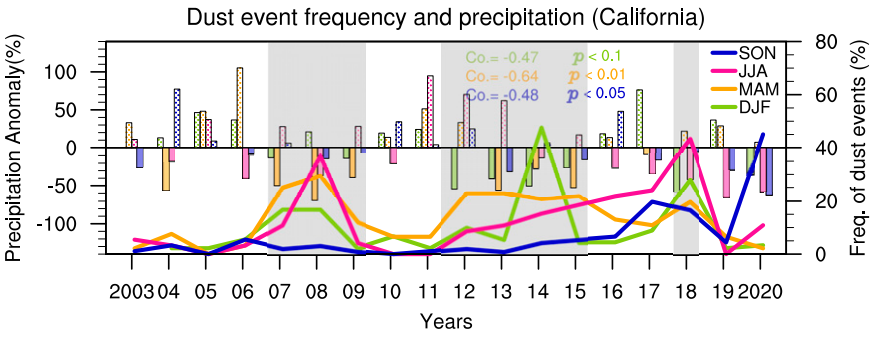

FIG. 1. Dust event frequency and precipitation anomaly in California, showing time series of the dust event frequency (number of dusty days divided by total number of days of each season, in percent; lines) from MODIS and precipitation anomaly (in percent with reference to the 2003–20 climatology; bars) from PRECL for each season (green for winter, orange for spring, magenta for summer, and navy for autumn). Recent drought years are shaded in gray. Correlation coefficients between precipitation and dust event frequency above the 95% confidence level (*t* test) are listed (with the color denoting the season).

2. Background

a. California drought and heat wave

California droughts usually lie within a large-scale context of droughts in the southwestern United States (Seager 2007; Hoerling et al. 2010; Seager et al. 2015), where drought is a "normal part of climate" (Weiss et al. 2009). The underlying mechanism of drought development is not completely understood, but modeling study indicates that tropical Pacific Ocean sea surface temperature (SST) controls about one-quarter of the interannual variability of precipitation in the Southwest (Seager and Hoerling 2014). An observational study found that wet conditions in California tend to occur during El Niño events, while dry conditions are more related to a North Pacific–North American wave train without obvious SST forcing (Seager et al. 2015). Overall, SST anomalies drive up to one-third of California wet season precipitation variance, with random atmospheric variability being an additional contribution.

A heat wave, defined as an event with consecutive extremely hot days, is another type of climate extreme that affects the economy, public health, and ecosystem in California (Knowlton et al. 2009; Gershunov and Guirguis 2012; Clemesha et al. 2018). The 2006 heat wave over California's Central Valley cost about $1 billion in the dairy industry alone (Bilby et al. 2008). Heat waves in California have been related to anomalous atmospheric circulation changes, such as reduced sea level pressure, anomalous easterly wind, and anomalous height at 500 hPa over the northwest coast (Lau and Nath 2012). Offshore Santa Ana winds (Raphael 2003), which are dry and hot easterly or northeasterly winds blowing from the deserts that usually occur in autumn and winter and favor wildfires (Westerling et al. 2004; Conil and Hall 2006; Hughes and Hall 2010), can sometimes cause California coastal heat waves (Gershunov et al. 2009; Gershunov and Guirguis 2012). In addition, land surface conditions, such as soil moisture, land use change, and irrigation, may affect heat waves as well (Perkins 2015; Grotjahn et al. 2016).

California's Central Valley is one of the most agriculturally productive regions and home to more than 5 million people (Grotjahn 2011). Heat waves in the region have been extensively studied. The development of Central Valley heat waves is associated with multiple factors, such as adiabatic heating due to subsidence, radiative heating under clear sky, and warm advection (Grotjahn 2011; Horton et al. 2016; Palipane and Grotjahn 2018), while the onset of a heat wave is related to a ridge–trough–ridge pressure pattern across the North Pacific and western North America (Grotjahn 2011; Lee and Grotjahn 2016; Grotjahn and Lee 2016).

The temperature and precipitation extremes are closely related to each other via land–atmosphere interactions. Drought favors temperature extremes (Hirschi et al. 2011; Schubert et al. 2014; Mueller and Seneviratne 2012), as reduced soil moisture prohibits cooling through evapotranspiration (e.g., Zaitchik et al. 2006; Jaeger and Seneviratne 2011). On the other hand, high temperature further enhances evaporation from soil and intensifies droughts (e.g., Trenberth et al. 2014). Studies found that droughts are more than twice as likely to occur when the California precipitation deficit is accompanied by warm conditions (Diffenbaugh et al. 2015). Understanding conditions favorable for concurrent drought and heat waves will help provide useful information for reliable projections.

b. Dust pollution in California and drought

Mineral dust is lifted to the atmosphere from dry and sparsely vegetated surface by wind. It absorbs and scatters both solar and terrestrial radiation and thus influences a wide range of atmospheric and environmental processes (e.g., Cook et al. 2009; Zhao et al. 2012; Painter et al. 2010). Dust particles also affect air quality. Over the southwestern and central United States, fine dust (with an aerodynamic diameter <2.5 μm) contributes about 20%–50% to total $PM_{2.5}$ mass in spring and summer (Hand et al. 2017). Severe dust storms degrade visibility and cause breathing problems and lung diseases, endangering public transportation and health (e.g., Kolivras and Comrie 2004; Goudie 2009; Schweitzer et al. 2018; Crooks et al. 2016). Incidences of "valley fever" (caused by a soil-dwelling fungus)

Brought to you by NOAA Central Library | Unauthenticated | Downloaded 07/19/23 05:08 PM UTC

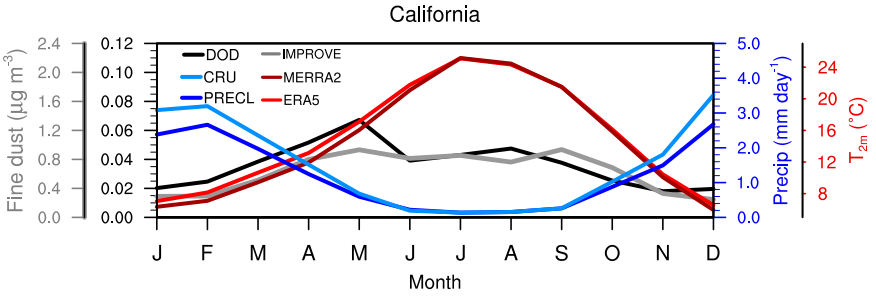

FIG. 2. Seasonal cycle of monthly precipitation (light and dark blue; mm day^{-1}), 2-m temperature (red and dark red; °C), DOD (black), and surface fine dust concentrations (gray; μg m^{-3}) from different datasets averaged over California for 2003–20.

in California and Arizona are also associated with dust storms (e.g., Zender and Talamantes 2006; Tong et al. 2017).

Major dust sources in the United States are located over the southwestern and the central United States (Prospero et al. 2002; Ginoux et al. 2012). Over California, dust sources are largely located in the central and southeastern parts of the state, including the Mojave and Sonoran Deserts in the southeast and croplands in the Central Valley (Clausnitzer and Singer 1996; Gill 1996; Chow et al. 1992, 2003). Desiccated lakes, such as Owens Lake and Mono Lake, are also local dust sources (Ginoux et al. 2012). In addition, trans-Pacific Asian dust is found along the U.S. West Coast in spring (e.g., VanCuren and Cahill 2002; Fischer et al. 2009; Yu et al. 2012; Creamean et al. 2014; Yu et al. 2019; Kok et al. 2021).

Despite different origins of dust, studies found that interannual variations in overall dustiness and surface fine dust concentrations in the southwestern United States, including California, are largely influenced by local precipitation, surface wind speed, and vegetation coverage (Pu and Ginoux 2017, 2018a) that affect dust emissions, transport, and deposition (e.g., Fécan et al. 1999; Gillette and Passi 1988; Zender and Kwon 2005; Jin et al. 2021). Surface winds lift dust from surface and transport it away from source regions, while precipitation removes small dust particles in the atmosphere by scavenging and also increases soil moisture, which enhances soil cohesion and prevents wind erosion. Vegetation increases surface roughness and reduces near-surface winds; its shade and root system help sustain soil moisture (e.g., Raupach 1994; Zender et al. 2003), limiting dust emissions.

Precipitation deficit increases surface fine dust concentrations and overall dustiness in the southwestern United States (Hand et al. 2017; Achakulwisut et al. 2017; Borlina and Rennó 2017; Pu and Ginoux 2017, 2018a). Such a connection between drought and dust emissions has long been noticed in different regions, but to our best knowledge it has not been thoroughly studied in California. What factors affect dust emissions during severe droughts? Does dustiness increase during California heat wave events? We will explore these questions in the following analysis.

c. Compound events

Extreme events can occur simultaneously or sequentially in the same location. Here we refer to the concurrent extreme events as compound events. Concurrent heat wave and drought events are reported in California (AghaKouchak et al. 2014), while enhanced dust pollution during dry periods is also noticed (Borlina and Rennó 2017). However, little is known about the features and mechanisms of concurrent drought, heat wave, and dust pollution events in California. California has a mild, dry summer and a wet winter from November to April (Fig. 2). Dust activities peak in spring and summer while temperature maximizes in summer. Therefore, we focus on compound events during March–August, when dustiness and temperature are high and the precipitation rate is relatively low. We will first identify (section 3) and characterize (section 4a) concurrent drought, heat wave, and dust events in California and then examine the favorable large-scale conditions for the development of compound events (section 4b). We also examine air quality conditions during compound events (section 4c) and compare compound events with California heat waves (section 4d). Major conclusions are summarized in section 5.

3. Data and method

a. Datasets

The following datasets are used to identify compound events and characterize their spatial and temporal features and examine conditions associated with their development.

1) PRECIPITATION

Monthly precipitation data from the Climatic Research Unit (CRU) time series (TS) 4.05 (Harris and Jones 2020), available from 1901 to 2020 on a 0.5° × 0.5° grid, are used to select drought years of California. The gridded data are based on the analysis of over 4000 individual weather station records. Precipitation Reconstruction over Land (PRECL; Chen et al. 2002) from the National Oceanic and Atmospheric Administration is a global analysis available monthly from 1948 to present at a 1° × 1° resolution. Precipitation from PRECL is also used for a comparison.

Daily precipitation from the Integrated Multi-satellitE Retrievals for GPM (IMERG) Final product (level 3, version 6; Huffman et al. 2019) on a 0.1° × 0.1° grid from 2003 to 2020 is used for composite analysis. IMERG is a multisatellite product using both backward and forward morphing schemes and is calibrated by Global Precipitation Climatology Centre (GPCC) monthly gauge analysis. IMERG precipitation has

Brought to you by NOAA Central Library | Unauthenticated | Downloaded 07/19/23 05:08 PM UTC

been extensively validated against ground observations globally and over the United States (e.g., Tan et al. 2016; Dezfuli et al. 2017; Xu et al. 2017; Tan et al. 2017; Sungmin and Kirstetter 2018; Cui et al. 2020; Wang et al. 2021). It shows good correlations with local gauge observations in case studies in California but underestimates overall magnitude (Wen et al. 2018). Sungmin and Kirstetter (2018) suggested that IMERG precipitation can be "a reliable alternative to ground-based measurements" in the United States, although region-specific data discrepancies exist. They found that diurnal variations in precipitation are underestimated over mountainous regions in the western and eastern United States. The dataset also tends to underestimate high-end extreme precipitation rates (Li et al. 2022).

2) TEMPERATURE

Surface 2-m temperatures from the European Centre for Medium-Range Weather Forecasts (ECMWF) reanalysis ERA5 (Hersbach et al. 2020) from 1980 to 2020 are used to identify and characterize California heat waves. ERA5 is the latest reanalysis product from ECMWF, which provides hourly variables on an about 31-km resolution. Ground-based surface temperature observations are assimilated to ERA5 via its land data assimilation system (Hersbach et al. 2020). The dataset has been used to study heat extremes in North America (Thompson et al. 2022), Europe (Dirmeyer et al. 2021; Gouveia et al. 2022), and globally (e.g., Freychet et al. 2021; Rogers et al. 2022; Awasthi et al. 2022; Zhang et al. 2022). Daily maximum temperature T_{max} is calculated from hourly data. Monthly 2-m temperatures from ERA5 and from the Modern-Era Retrospective Analysis for Research and Applications, version 2 (MERRA-2; Gelaro et al. 2017), are used to examine the seasonal cycle to identify compound events. Daily sea surface temperature from ERA5 is used to examine SST anomalies associated with compound events.

3) DUST AND $PM_{2.5}$ CONCENTRATIONS

Dust optical depth (DOD) is column-integrated extinction by mineral particles and describes overall dustiness. Daily DOD is retrieved from Moderate Resolution Imaging Spectroradiometer (MODIS) Deep Blue aerosol products (Collection 6.1, level 2; Sayer et al. 2019) using aerosol optical depth (AOD), single-scattering albedo, and the Ångström exponent (Yu and Ginoux 2021). Note since DOD is a column-integrated variable, it contains dust from both local emissions and remotely transported dust, although the latter is often smaller near dust source regions. MODIS DOD products have been used to identify and characterize dust sources (Ginoux et al. 2012; Baddock et al. 2016) and examine the variations in dustiness in different regions (e.g., Pu and Ginoux 2016, 2017, 2018b). Daily MODIS DOD from the *Aqua* satellite (passing the equator at 1330 local time) on a $0.1° \times 0.1°$ grid is available from 2003 to 2020, so our study also focuses on 2003–20. The climatology of DOD in March–May, June–August, and the March–August average along with data availability are shown in Fig. S1 in the online supplemental material. During spring and summer, most of the study area has a data coverage of more than 50% of the total number of days.

Dust source regions are identified following Ginoux et al. (2012) using frequency of occurrence (FoO), which is the number of days when daily DOD > 0.2 divided by the total number of days. Note that while there are uncertainties associated with dust source detection via polar-orbiting satellite products due to their relatively low temporal coverage (Schepanski et al. 2012), studies found that high DOD tends to appear more frequently over source regions, even in windy regions such as the Bodélé depression (Ginoux et al. 2010, 2012). Here we focus on March–August. Only regions where MODIS normalized difference vegetation index (NDVI) < 0.25 (i.e., sparsely vegetated regions) are considered as dust sources following Vukovic et al. (2014). Results are similar if using a threshold of leaf area index less than 0.3. We further separate dust sources into natural and anthropogenic sources following Ginoux et al. (2012). Yearly land use from the History Database of the Global Environment (HYDE), version 3.2 (Goldewijk et al. 2017), on a $\sim 0.08° \times 0.08°$ grid from 2003 to 2015 is used. Dust source regions with agricultural land use (croplands and pasturelands) greater than 30% are considered anthropogenic. In addition, we further mask out the dust source regions with irrigation area >30% using the MODIS Irrigated Agriculture Dataset for the United States (MIrAD-U.S.; Pervez and Brown 2010; Brown and Pervez 2014) on a 1-km resolution (interpolated to $0.1° \times 0.1°$ grids). In warm-season California, anthropogenic dust sources are mainly over croplands and pasturelands in the Central Valley associated agricultural activities, while natural dust sources are located over the southeastern area dominated by deserts and open shrublands (Fig. 3). The identified dust source region largely resembles that detected by Ginoux et al. (2012, their Fig. 11). A recent study found that DOD with a low-quality flag (i.e., QA = 1) had better performance in detecting dust sources than that with a high-quality flag (i.e., QA = 3), because retrieved aerosol products were often poorly flagged over dust source regions (Baddock et al. 2016). Dust sources identified using DOD flagged with QA = 1 are shown in Fig. S2 in the online supplemental material. In general, larger source region over eastern California and higher FoO are found.

Surface fine dust concentrations from the Interagency Monitoring of Protected Visual Environments (IMPROVE) network are used. IMPROVE has collected near-surface $PM_{2.5}$ samples in the United States since 1988 (Malm et al. 1994; Hand et al. 2011). IMPROVE stations are located in national parks and wilderness areas, and $PM_{2.5}$ sampling is performed twice weekly (Wednesday and Saturday; Malm et al. 1994) prior to 2000 and every third day afterward. This dataset has been widely used to study variations in surface fine dust in the United States (e.g., Pu and Ginoux 2018a; Hand et al. 2017; Tong et al. 2017; Pu and Jin 2021). Here daily data from 2003 to 2019 are used to form composites of compound events.

The U.S. Environmental Protection Agency (EPA) Air Quality System (AQS) dataset provides outdoor air quality data across the United States, Puerto Rico, and the U.S. Virgin Islands. Daily $PM_{2.5}$ concentrations from AQS from 2003 to 2019 are used to examine the air quality impacts of compound events.

4) LAND SURFACE VARIABLES

Hourly surface volumetric soil moisture from ERA5 in the first layer (0–7 cm) is used to calculate daily data to

Brought to you by NOAA Central Library | Unauthenticated | Downloaded 07/19/23 05:08 PM UTC

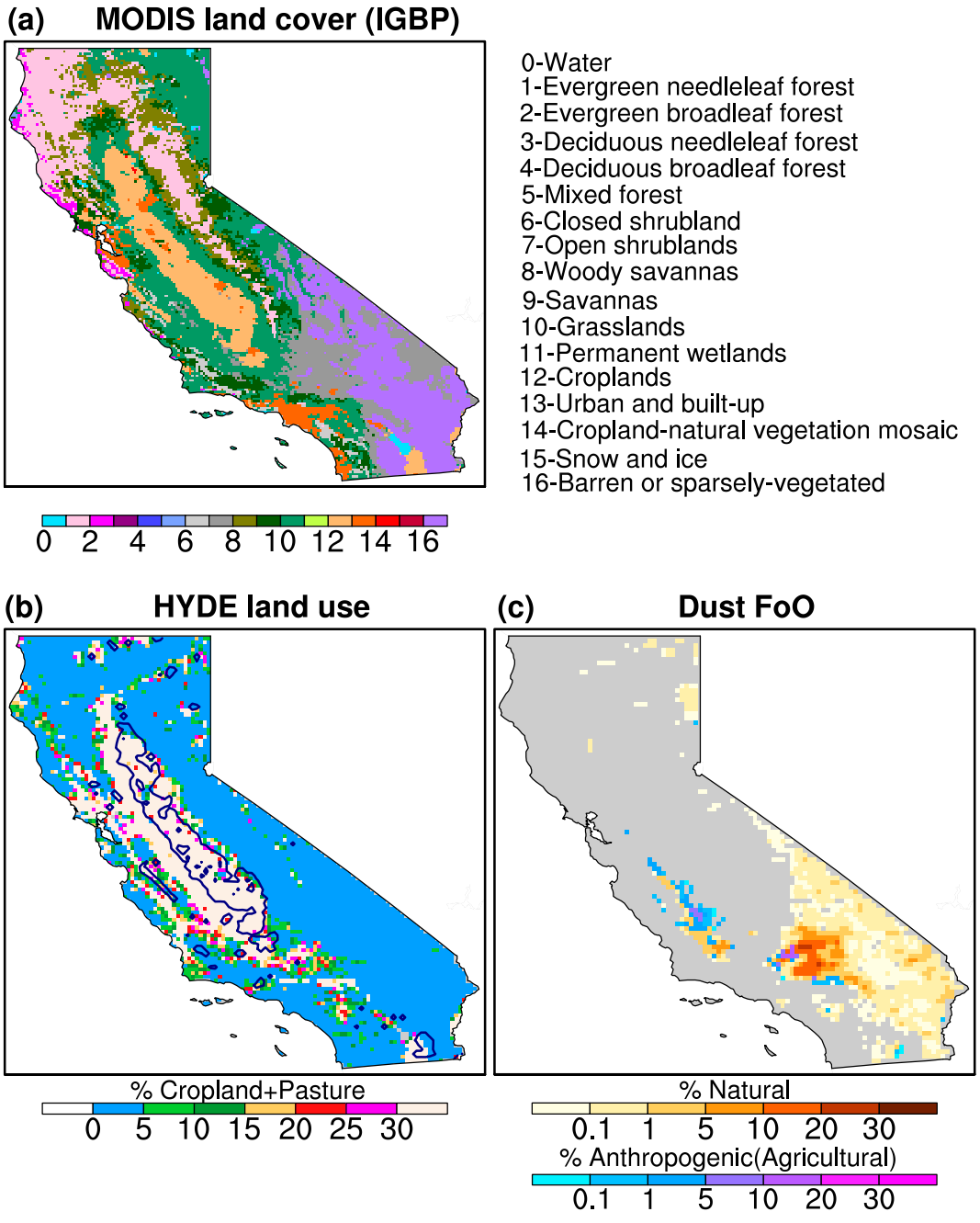

FIG. 3. (a) MODIS land cover type (each grid shows the dominant land cover type during 2003–19). (b) HYDE land use (area of croplands and pasturelands divided by the total area of each land grid; %) averaged over 2003–15. (c) Dust frequency of occurrence (FoO; see the definition in the text) for March–August. Natural dust sources are shown in brown shading, and anthropogenic dust sources are in blue to purple shading. Blue contours in (b) denote regions with irrigation rate greater than 30% from MIrAD-U.S. average.

examine land surface conditions associated with compound events. Scatterometer soil moisture from Active Microwave Instrument (AMI) on European Remote Sensing Satellites 1 and 2 (*ERS-1*, *-2*) from 1991 to 2006 and Advanced Scatterometer (ASCAT) aboard Meteorological Operational Satellites A and B (*MetOp-A*, *-B*) from 2007 to 2014 are assimilated into ERA5 (Hersbach et al. 2020). ERA5 soil moisture shows high skill in comparison with station observations (Li et al. 2020). Over the United States and Europe, its temporal correlations with in situ soil moisture measurements are comparable to or higher than several satellite products (Beck et al. 2021).

Brought to you by NOAA Central Library | Unauthenticated | Downloaded 07/19/23 05:08 PM UTC

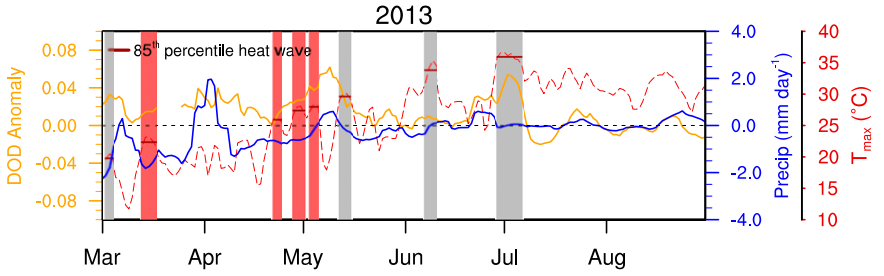

FIG. 4. Concurrent California drought, heat wave, and dust events (i.e., compound events) in 2013. Orange and blue lines denote anomalies (with reference to the 2003–20 mean) of daily DOD and precipitation (smoothed by 7-day running mean), respectively. The red dashed line shows daily maximum temperature T_{max}. Horizontal dark red lines show averaged T_{max} during heat waves defined by the 85th-percentile threshold (see the text). Heat waves are highlighted by vertical shading (eight in total), with red shading denoting compound events.

The level-3 monthly NDVI retrieved from *Terra*-MODIS on a resolution of 0.1° × 0.1° (Collection 6; Didan 2015a,b) is used to examine land surface condition associated with compound events. NDVI represents the density of green vegetation, ranging from −1 to 1. Over land the lower boundary is near zero and the upper boundary approximates 0.8 (Huete et al. 1999), with higher values indicating greater density of green vegetation. We linearly interpolate 16-day NDVI into daily data on a resolution of 0.25° × 0.25° to form daily composites of compound and heat wave events. Yearly MODIS land cover type (MCD12C1) on a 0.05° × 0.05° grid from 2003 to 2019 is used to examine land cover.

5) ATMOSPHERIC CIRCULATION

Meteorological variables such as daily and monthly 850- and 500-hPa winds and geopotential heights from the ERA5 are used to examine circulation patterns associated with the development of compound events.

b. *Definition of compound extreme events*

To examine the characteristics of concurrent drought, heat wave, and dust events, we define a compound event when it meets the following criteria during spring and summer (March–August): (i) within a drought year of California, (ii) days within a California heat wave, (iii) days within a dusty season of California and within these days at least two-thirds of days with positive DOD anomaly. Each of the criteria is explained in detail as follows. We select March–August largely based on seasonal variations in DOD, surface temperature, and precipitation (Fig. 2). DOD describes total light extinction by column dust aerosols regardless of size, and thus is more suitable to represent overall dustiness. It is also one of the key variables controlling dust–radiation interactions (single-scattering albedo and asymmetry factor being the two others). The selected period also partially covers the secondary peak of surface fine dust concentrations in the Sierra Nevada area in August–September (Hand et al. 2017; see their Fig. 5).

A drought year is defined when the 6-month standard precipitation index (SPI-6) in April is equal or less than −0.6 for California. SPI has been widely used to define drought, and SPI-6 in April reveals precipitation deficit from November to April, covering the main rainy season in California. Monthly precipitation data from CRU TS 4.05 from 1980 to 2020 is used to calculate SPI-6 in California. Eight drought years are found during 2003–20: 2007–09, 2012–15, and 2018. The identified drought years are consistent with previous studies of California droughts (e.g., Seager et al. 2015).

A heat wave is usually defined as a few consecutive days with temperature greater than certain threshold, either percentile-based or a fixed value (e.g., Grotjahn et al. 2016; Zhang et al. 2020). Here we use values of the 85th percentile of regional averaged daily T_{max} in California from ERA5, centered over a 15-day window (Perkins and Alexander 2013), during March–August from 1980 to 2020 as thresholds (i.e., each day, the 85th percentile of T_{max} is calculated among 15 × 41 days). Using such as a moving window increases sample size and also accounts for temporal variations of surface temperature (Perkins and Alexander 2013). A heat wave is defined when regional averaged T_{max} exceeding the threshold and lasting at least three consecutive days. We found 100 heat wave events in warm seasons during 2003–20.

A dusty season is defined as the dust event frequency (number of dusty days divided by the total number of days of the season, in percentage) in a season being greater than 20%. A dusty day is when the daily DOD anomaly (with reference to climatological mean) is greater than one standard deviation (Pu and Ginoux 2017). Since DOD may contain missing values in the area that affects the analysis, we select events only when daily DOD spatial coverage in California is ≥30% for at least two days during each event.

Since the MODIS DOD is available from 2003 to 2020, our analysis of California compound events also focuses on this time period. Figure 4 shows the heat waves and compound events identified in a drought year in 2013 as an example. We found eight heat waves (shading), and among them four are compound events (red shading). In total, 16 compound events of 60 days are identified during 2003–20. While looser criteria of compound events probably would result in more events, we argue that these relatively strong events show the worst-case scenarios of concurrent drought, heat wave, and dusty

Brought to you by NOAA Central Library | Unauthenticated | Downloaded 07/19/23 05:08 PM UTC

TABLE 1. List of California compound events and corresponding anomalies (with reference to the 2003–20 mean). Values in parentheses in the last two columns are magnitudes of anomalies in comparison with the March–August mean over 2003–20 (%).

Events	Year	Dates	Duration (days)	T_{max} anomaly (°C)	Precipitation anomaly (mm day^{-1})	DOD anomaly
1	2007	27–29 Apr	3	5.52	−0.55 (−80.1%)	0.03 (53.3%)
2	2008	12–14 Apr	3	6.73	−1.14 (−166.1%)	−0.01 (−10.6%)
3	2008	15–20 May	6	7.79	−0.81 (−118.2%)	0.03 (51.1%)
4	2008	19–22 Jun	4	3.49	0.07 (9.8%)	0.02 (33.5%)
5	2008	7–10 Jul	4	3.73	−0.08 (−12.1%)	0.09 (157.6%)
6	2008	14–16 Aug	3	2.29	−0.08 (−12.1%)	0.04 (69.9%)
7	2012	20–23 Apr	4	6.51	−0.74 (−107.0%)	0.00 (1.8%)
8	2013	12–16 Mar	5	4.51	−1.68 (−244.6%)	0.02 (33.0%)
9	2013	21–23 Apr	3	4.84	−0.76 (−110.0%)	0.02 (27.6%)
10	2013	27–30 Apr	4	5.08	−0.51 (−73.7%)	0.02 (44.4%)
11	2013	2–4 May	3	4.68	−0.61 (−88.5%)	0.05 (97.3%)
12	2014	25–27 May	3	5.86	−0.66 (−95.7%)	0.00 (6.0%)
13	2018	17–19 Jul	3	2.35	−0.00 (−0.1%)	0.03 (48.2%)
14	2018	24–29 Jul	6	2.60	−0.07 (−10.7%)	0.08 (138.9%)
15	2018	8–10 Aug	3	3.42	−0.10 (−13.9%)	0.14 (258.2%)
16	2018	18–20 Aug	3	1.77	−0.14 (−20.6%)	0.06 (107.8%)
Mean			3.75	4.45	−0.49 (−71.5%)	0.04 (69.9%)

conditions that better reveal the characteristics of compound events. We test the sensitivity of the above thresholds using the 80th percentile of T_{max} for heat waves and 15% for dusty seasons, and 18 events of 80 days are found, with similar patterns of composites but slightly smaller magnitude of temperature and DOD anomalies (not shown). We also tested using DOD over dust source regions (Fig. 3c) to calculate dusty seasons and found 27 events, largely due to higher daily DOD values over the sources. Correspondingly, compound events show higher values of DOD anomalies over the sources in southern California as expected, while other features are generally similar to the findings here.

4. Results

a. *Features of compounding drought–heat wave–dust events in California*

Table 1 lists the 16 compound events during 2003–20, with durations ranging from 3 to 6 days. The average duration is about 4 days. During compound events, regional-averaged T_{max} increases by 1.77°–7.79°C, with a mean warming of 4.45°C, with reference to the 2003–20 climatological mean. Precipitation on average decreases by about 0.5 mm day^{-1}, and DOD increases by about 0.04 (~70% of their 2003–20 climatological means over March–August; Table 1).

We then average among all the days of compound events to form composites. Figures 5a–c show the spatial pattern of 2-m temperature, precipitation, and DOD from the composites. Anomalous warming is largely located over northern to central California (Fig. 5a), with precipitation deficits mainly over northern California (Fig. 5b; note that precipitation rate is climatologically low over southern California). Such a dry condition in California is associated with precipitation reduction over the whole western United States, especially over the northwest coast and Montana (Fig. S3b in the online supplemental material). The warming is also not limited to California but rather occurs over large parts of the western United States (Fig. S3a), indicating that temperature and precipitation anomalies are associated with large-scale features instead of local systems. DOD increases over central to southern California, with the highest anomalies over natural dust sources in the south (Fig. 5c). Meanwhile, DOD over major dust sources in the southwestern United States, such as the Colorado Plateau, the Great Basin deserts, and the Sonoran and Chihuahuan Deserts, are not significantly enhanced (Fig. S3c), also indicating that the enhanced DOD in California dust source regions is largely associated with local emissions.

Daily mean surface wind speed slightly decreases (0.4–0.6 m s^{-1} and up to 1 m s^{-1} at a few grids), with anomalous northerly winds over northern California, easterly winds over large parts of southern California, and southeasterly to northeasterly winds converging over the Central Valley (Fig. 5d). The anomalous surface winds favor the transport of enhanced dust from inland deserts and anthropogenic sources (Fig. 3c) to central and western California and increase DOD (Fig. 5c). Over the southwestern United States, the easterly wind anomalies bring dry air downslope from the Rocky Mountains and Sierra Nevada (supplemental Fig. S3d), a pattern that promotes heat waves in the Pacific Northwest and California (Lau and Nath 2012).

Soil moisture anomalies generally follow precipitation deficits, with the largest reduction in northern California extending toward the Central Valley (Fig. 5e). Reduced soil moisture decreases latent cooling, favoring the development of heat waves. Note that irrigation over croplands can perturb the natural water cycle and may suppress dust emissions from anthropogenic sources. Although ERA5 assimilates satellite scatterometer soil moisture, its capability in representing irrigation induced soil water change in the United States is not clear. Studies found that during severe drought years, irrigation (through additional

Brought to you by NOAA Central Library | Unauthenticated | Downloaded 07/19/23 05:08 PM UTC

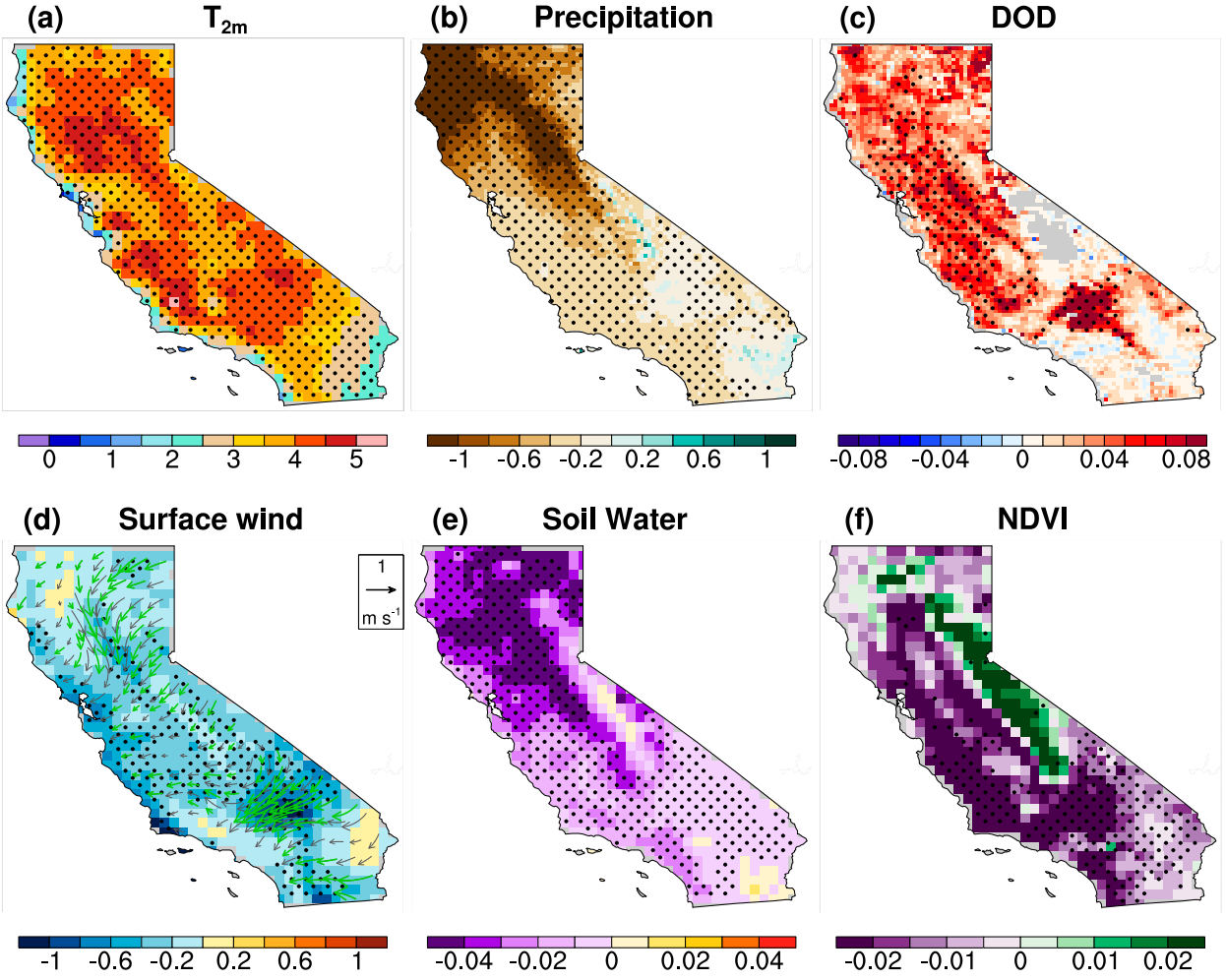

FIG. 5. Daily composites of California compound events: (a) 2-m temperature (°C), (b) precipitation (mm day^{-1}), (c) DOD, (d) surface wind speeds (shading; m s^{-1}) and direction (vectors), (e) soil moisture (m^3 m^{-3}), and (f) NDVI anomalies (with reference to the 2003–20 mean). The area significant at the 95% confidence level (*t* test) is stippled. Surface winds significant at the 95% confidence level are plotted as green vectors.

groundwater pumping) cannot fully meet the water use demand, and methods such as fallowing, idling, and stress irrigation are applied to mitigate water shortage in California (Lund et al. 2018). This is generally consistent with the overall surface soil moisture reduction shown in ERA5 (Fig. 5e). Using the MIrAD-U.S., we also found that overall irrigation area in drought years of 2007 and 2012 slightly decreased from a normal year of 2002 (Fig. S4 in the online supplemental material). A full quantification of how irrigation may affect compound events is outside the scope of this paper but warrants future studies.

Persistent soil moisture deficit during a drought and high air temperature both exert negative impacts on vegetation. NVDI decreases in large area of California, with the greatest reduction over central, western, and parts of southern California (Fig. 5f), where NDVI absolute values are generally less than 0.3 (not shown). These regions are largely covered by grasslands, cropland, and open shrublands, or sparsely vegetated (Fig. 3a), and are nearly collocated with dust sources (Fig. 3c). Low NDVI (e.g., less than 0.25; Vukovic et al. 2014) is usually considered as susceptible to wind erosion. Reduced NDVI along with soil moisture deficit in dust source regions in southern California tends to promote dust emissions, despite a weak reduction of total wind speed. Areas with severe NDVI reduction are generally collocated with the regions with large increase in DOD (Fig. 5c), indicating that vegetation decay plays an important role in enhancing dust emissions.

b. *Favorable large-scale conditions associated with compound events*

In this section we examine atmospheric circulation and SST patterns associated with the compound events to better understand their formation. Figure 6 shows daily composites of 850- and 500-hPa geopotential height and wind anomalies during compound events. In the lower troposphere, an anomalous high is centered off the west coast around 40°–50°N,

Brought to you by NOAA Central Library | Unauthenticated | Downloaded 07/19/23 05:08 PM UTC

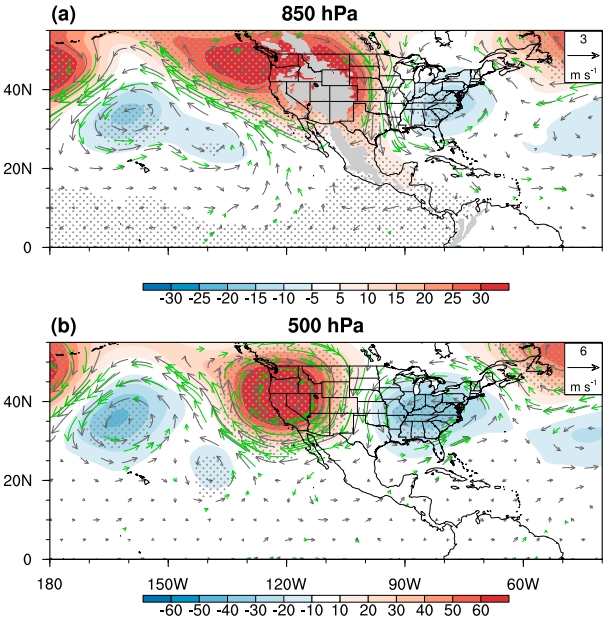

FIG. 6. Composites of (a) 850- and (b) 500-hPa wind (m s^{-1}) and geopotential height (gpm) anomalies during California compound events. The area significant at the 95% confidence level (*t* test) is stippled. Winds significant at the 95% confidence level are plotted as green vectors. Topography is masked out in gray.

extending toward the eastern North Pacific (Fig. 6a). The circulation pattern at 500 hPa largely resembles that at 850 hPa (Fig. 6b), with an anomalous high sitting over the northwest coast around 45°N. Both California droughts and heat waves have been related to the anomalous high at the west coast, although in different seasons (i.e., winter during droughts and warm season in heat waves) (e.g., Lau and Nath 2012; Seager et al. 2015; Grotjahn and Faure 2008; Grotjahn 2011; Clemesha et al. 2018). Here the anomalous sinking motion associated with the high pressure system not only favors subsidence and dry condition in spring and summer, but also can warm the lower troposphere by adiabatic heating. The anomalous easterly winds on the other hand can suppress the cooling sea breezes from ocean, also supporting the development of heat waves (Grotjahn 2011; Lee and Grotjahn 2016; Grotjahn and Lee 2016; Grotjahn et al. 2016).

Figure 7 shows the evolution of circulation patterns associated with the development of compound events, from seven (day −7), five (day −5), and three (day −3) days before to the first day (day 0) of compound events. The anomalous high off the U.S. West Coast is part of a ridge–trough–ridge pattern over the North Pacific that starts to develop up to seven days before the events (Figs. 7d,h). The anomalous high over the Gulf of Alaska slowly moves eastward and appears over the U.S. West Coast about three days before compound events (Figs. 7b–d,f–h). A nearly stationary ridge–trough–ridge wave train has been related to California heat waves in previous studies (e.g., Lee and Grotjahn 2016; Grotjahn and Lee 2016; Lau and Nath 2012). Here we found this circulation pattern is also evident in compound events. The strengthening of the height anomaly over the west coast about 3 days prior to compound event onset is somewhat similar to the evolution of circulation patterns associated with the cluster-1 Central Valley heat waves (Lee and Grotjahn 2016), although here the coastal high does not develop from a weak ridge west of California and the zonal wavelength of the wave train is a bit longer.

Previous studies suggested that the connection between California droughts and SST is generally weak, although a few droughts have been related to SST anomalies, such as the 2011/12 drought to La Niña, and the 2012–14 drought to a warm west and cold east SST dipole pattern over the tropical Pacific (Seager et al. 2015). Are compound events associated with any specific SST patterns? Figure 8 shows the composites of SST from seven days before compound events to the onset of the events. A weak negative SST anomaly (SSTA) is found over the western to central topical Pacific between 150°W and 150°E, somewhat resembling a cold phase of the Pacific decadal oscillation but with a weak positive SSTA over the eastern tropical Pacific (Fig. 8). The pattern persists for at least a week until the onset of compound events. Among the six drought years with compound events, four of them (2007, 2008, 2012, and 2018) experience La Niña in part of the warm season (March–August), likely contributing to the weak cooling over the western to central tropical Pacific in the composites (Fig. 8).

The tropical SSTA could reveal variability in shorter time scales associated with California heat waves as well. Part of the anomalous cooling of tropical western Pacific SST somewhat resembles the western Pacific intraseasonal oscillation (WPISO; Wang and Xie 1997) during its phases 3–7 in boreal warm season (May–October) (Yang et al. 2020, their Fig. 2), although the latter shows negative SSTA farther west and north, around 80°–160°E and 5°S–20°N. Phase 3–7 WPISO-induced Rossby waves can generate an anomalous high downstream over the western United States at 850 hPa and consequently increase surface air temperature over the western to central United States (Yang et al. 2020), which could favor the development of California heat waves. On the intraseasonal time scale, Madden–Julian oscillation (MJO) in phase-pairs 8–1 and 2–3 is also found to connect with the California Central Valley heat waves in summertime, when the MJO leads heat waves by about 2 weeks (Lee and Grotjahn 2019). The abovementioned MJO phases correspond to an anomalous high outgoing longwave radiation (OLR) and a transition from high to low OLR over the tropical western Pacific, which also modulate SST in the area (Zhang 2005), that is, a negative SSTA and a transition to positive.

In short, the tropical Pacific SSTA shown in the composite of compound events (Fig. 8) is likely a combination of signals on different time scale, such as a La Niña that favors California drought and anomalous cooling associated with WPISO and/or MJO phases that support California heat waves.

c. *Air quality impacts*

In addition to enhanced DOD and reduced precipitation during the compound events, subsidence associated with

Brought to you by NOAA Central Library | Unauthenticated | Downloaded 07/19/23 05:08 PM UTC

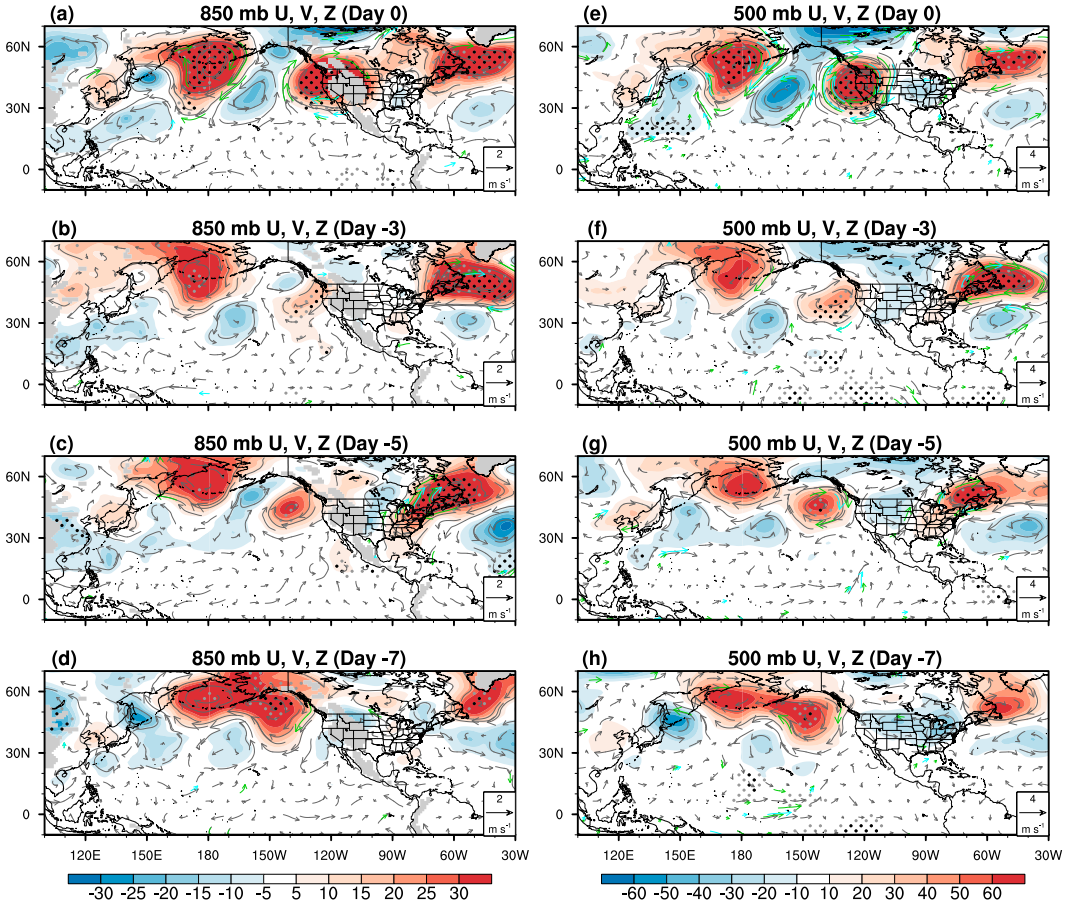

FIG. 7. Composites of (left) 850- and (right) 500-hPa wind (m s^{-1}) and geopotential height (gpm) anomalies from (d),(h) 7; (c),(g) 5; and (b),(f) 3 days before compound events (days −7, −5, and −3) and (a),(e) at the first day of compound events (day 0). Areas significant at the 90% and 95% confidence levels (*t* test) are stippled in gray and black, respectively. Winds significant at the 90% and 95% confidence levels are plotted as green and cyan vectors, respectively. Topography is masked out in gray.

anomalous high pressure over the West Coast tends to lower the subsidence inversion (e.g., Grotjahn 2011; Lee and Grotjahn 2016), all of which favor the accumulation of air pollutants in the area. Figure 9 shows the composites of surface fine dust and $PM_{2.5}$ concentrations during compound events. Consistent with the increase in DOD, we found surface fine dust concentrations enhance over large areas in California, with the greatest increase in central California by more than 0.5 μg m^{-3} (about 60%–70% of its climatological mean; Figs. 9a,c), which is partially associated with the wind convergence over the region (Fig. 5d). Surface fine dust also increases over northern California, Oregon, and Washington. Note that fine dust records are only available every three days, so the composite here may underestimate the total increase in fine dust concentrations in compound events.

Previous studies found that fine dust concentrations over the western United States are influenced by long-range transported dust from Asia, mostly in spring (e.g., VanCuren and Cahill 2002; Creamean et al. 2014; Hand et al. 2017). Elemental composition-based analysis (e.g., Fe/Ca ratio) also found that Asian dust concentrations in California sites are higher than those in Oregon and Washington (Creamean et al. 2014). However, a recent study using an observation-constrained inverse model suggests that Asian dust contributes less than 50% to annual mean DOD to the area south of 40°N over the western United States (including large parts of California) but more than 50% in the north (Kok et al. 2021). Separating local and transported dust is beyond the scope of this study; nonetheless, our analysis suggests that local dust likely dominates the variations in compound events given its close connection to local land surface conditions (see discussion in section 4d).

The $PM_{2.5}$ concentrations also increase over central California by more than 5 μg m^{-3} (up to 8 μg m^{-3}; Fig. 9b). The low topography of the Central Valley and surrounding mountains has been related to poor air quality during hot days in previous studies (Bao et al. 2008; Grotjahn 2011). In addition, extra energy consumption during heat waves and droughts (e.g., using natural gas instead of hydropower) can increase local anthropogenic emissions (Christian-Smith et al. 2011; Herrera-Estrada et al. 2018) and contribute to the increase in $PM_{2.5}$ particles. The

Brought to you by NOAA Central Library | Unauthenticated | Downloaded 07/19/23 05:08 PM UTC

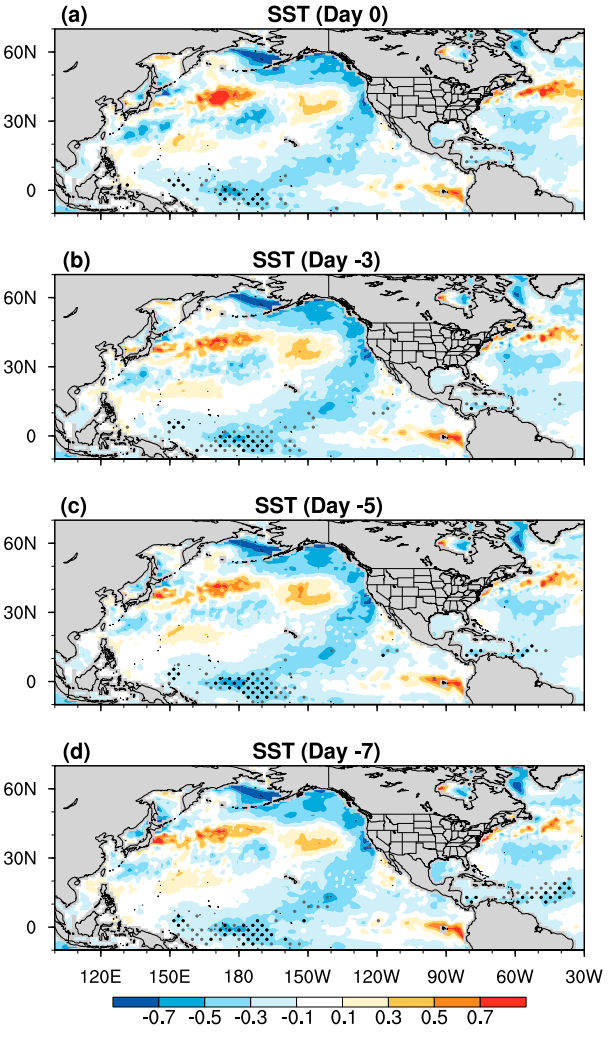

FIG. 8. Composites of SST anomaly (°C) (a) at the first day of compound events (day 0), and (b) 3 days, (c) 5 days, and (d) 7 days before compound events. Areas significant at the 90% and 95% confidence levels (*t* test) are stippled in gray and black, respectively.

degraded air quality may further exacerbate the health dangers associated with heat waves.

Wildfires could be another source of increased fine dust and $PM_{2.5}$ concentrations during compound events. Increased dust particles are found in smoke plumes (e.g., Gaudichet et al. 1995; Maenhaut et al. 1996; Kavouras et al. 2012; Nisantzi et al. 2014) and have been related to fire-induced circulation change that favor dust emissions (e.g., Wagner et al. 2021). In addition to coemissions, fire-induced land cover and soil properties changes (e.g., enhanced soil hydrophobicity) may increase surface erodibility and increase dust emissions after fires (Whicker et al. 2006; Ravi et al. 2007, 2012; Merino-Martín et al. 2014; Wagenbrenner et al. 2013, 2017; Dukes et al. 2018; Yu and Ginoux 2022). To clarify the potential influence of wildfires, we show MODIS fire counts summed over days of compound events, one week and two weeks before the days of compound events in Figs. S5a–c, respectively, in the online supplemental material. Fire count is derived from *Aqua* and *Terra* MODIS 1-km daily thermal anomalies and fire products during both day- and nighttime (MOD14A1 and MYD14A1; Collection 6.1) and remapped to a 0.1° × 0.1° grid. Over northern and central California, several sites with increased fine dust concentrations are close to fire spots (Fig. S5a) and thus are potentially affected by fire-induced dust emissions. Schlosser et al. (2017) found that fine dust concentrations increased by 22% during peak elemental-carbon days of 14 major wildfires in California from 2005 to 2015. Nonetheless, fine dust concentrations at sites nearby fire spots increased more than 70% during compound events (Fig. S5a; see also Fig. 9c), greater than the estimated increase due to fires (~22%), indicating that other factors, such as drought-enhanced dust emissions, play important roles in increasing surface dust concentrations. Similar fire patterns are found 1–2 weeks before the days of compound events (Figs. S5b,c). Fire-induced contemporary dust emissions are sensitive to the intensity, size, and duration of the fire (e.g., Wagenbrenner et al. 2017; Wagner et al. 2018), while post-fire emissions are affected by the soil properties, land cover, and vegetation recovery period (e.g., Ravi et al. 2012), and thus a detailed quantification of the contributions of wildfires to surface fine dust concentrations would require carefully designed numerical simulations with observation constraints, which falls beyond the scope of this paper.

d. *Compound events versus heat waves alone*

In this section, we compare compound events with heat wave events to further characterize their features. We select heat wave events in 10 nondrought years during 2003–20 (see the definition of California drought years in section 3b) given that dust emissions and droughts are closely linked. Composites are formed using all the 246 days of 48 heat wave events and are shown in Fig. 10. Surface 2-m temperature increases over northern, western, and southern California by 4.0°–4.5°C during heat waves (Fig. 10a), a pattern similar to compound events (Fig. 5a). Meanwhile, precipitation decreases over northern to central California (Fig. 10b), suggesting that dry conditions favor the development of heat waves. The spatial pattern of precipitation anomaly resembles that of compound events (Fig. 5b), but slightly wetter over northern California and drier over western central California. DOD changes little, with a slight decrease over the source region in southern California and a very weak increase over parts of the Central Valley (Fig. 10c).

Anomalous easterly surface winds are over large parts of California (Fig. 10d) and the southwestern to western United States (Fig. S6 in the online supplemental material), a pattern known to be associated with California heat waves. Consistent with precipitation deficit, soil moisture decreases over northern and western central California, but the overall magnitude is much weaker than that of compound events (Fig. 5c). NDVI on the other hand increases over parts of northern and southern California (Fig. 10f), likely contributing to the weak DOD decrease in southern California (Fig. 10c).

Figure 11 shows box plots that summarize the averaged daily 2-m temperature, precipitation, surface 10-m winds, soil moisture, and NDVI over California for compound events

Brought to you by NOAA Central Library | Unauthenticated | Downloaded 07/19/23 05:08 PM UTC

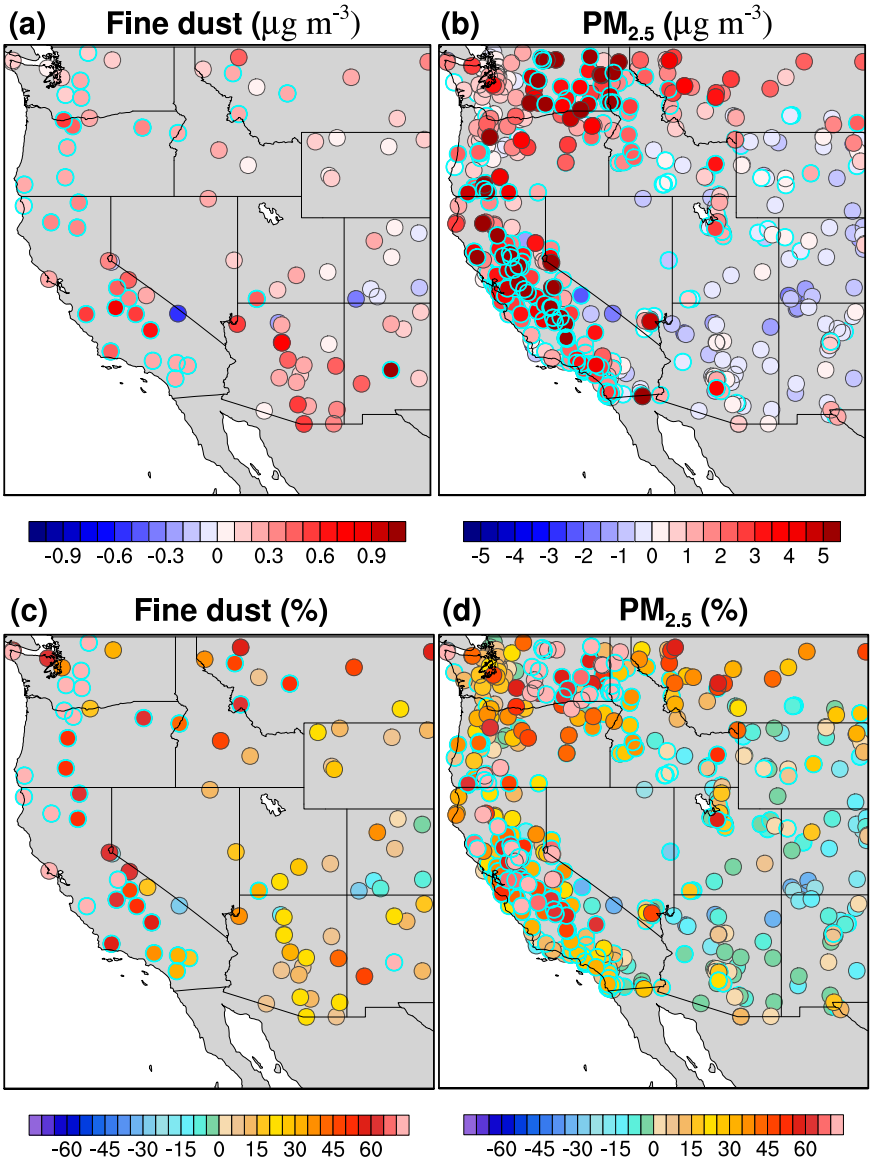

FIG. 9. Composites of anomalies of (a) surface fine dust and (b) $PM_{2.5}$ concentrations in absolute values ($\mu g\ m^{-3}$) during California compound events, and (c),(d) the same in percentage (%) of the 2003–19 mean over March–August. Station values significant at the 95% confidence level (*t* test) are marked by cyan-outlined circles.

(orange) and heat wave events (in nondrought years; red). The differences of mean temperature, precipitation, and surface wind speed between compound and heat wave events are not significant, although the range of precipitation anomalies in compound events is much smaller than that of heat waves (Figs. 11a,b,d). In association with persistent precipitation deficit, soil moisture and NDVI are significantly lower in compound events than heat waves, and DOD is significantly higher (Figs. 11e,f,c).

Previous studies suggest that heat wave concurrent with drought can intensify heat wave or drought alone (Zaitchik et al. 2006; Shukla et al. 2015; Perkins et al. 2012); however, such feedbacks are not evident in the comparison between compound and heat wave events. The maximum and minimum temperatures of compound events are slightly higher than those of heat wave events, but the mean and median are very similar (Fig. 11a). One possible reason is that feedbacks through land–atmosphere interactions (e.g., drier soil induced greater sensible heating and higher surface temperatures) are more evident in severe and long-lasting heat wave events, such as the 2003 summer heat wave in Europe (Zaitchik et al. 2006) but may be smoothed out in the composite average in observations. Modeling studies with controlled forcing (e.g., perturbed temperature or precipitation; Shukla et al. 2015) tend to show clearer signals of exacerbation.

Brought to you by NOAA Central Library | Unauthenticated | Downloaded 07/19/23 05:08 PM UTC

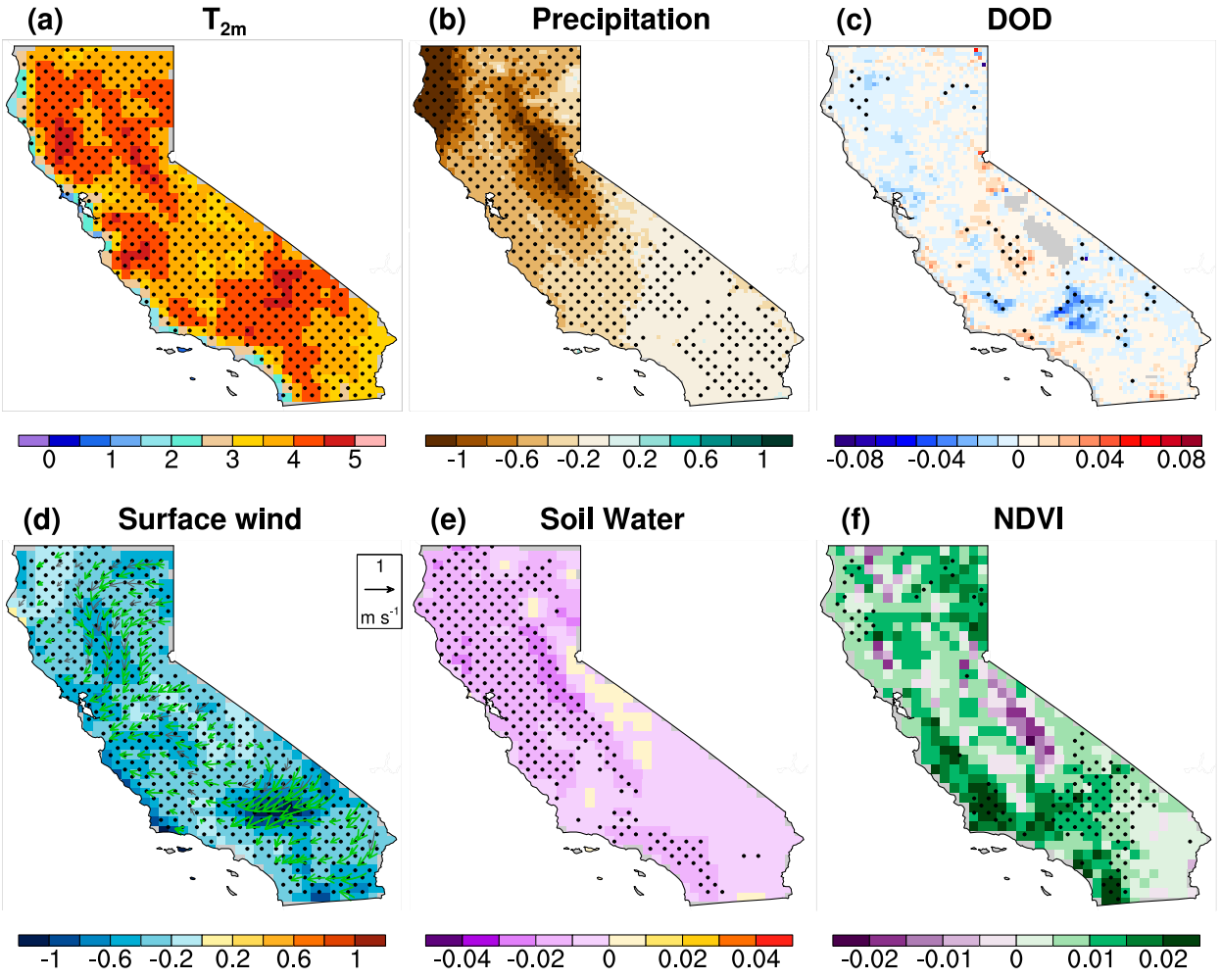

FIG. 10. Daily composites of California heat wave events in nondrought years: (a) 2-m temperature (°C), (b) precipitation (mm day^{-1}), (c) DOD, (d) surface wind speeds (shading; m s^{-1}) and direction (vectors), (e) soil moisture (m^3 m^{-3}), and (f) NDVI anomalies (with reference to the 2003–20 mean). The area significant at the 95% confidence level (*t* test) is stippled. Surface winds significant at the 95% confidence level are plotted as green vectors.

As shown in Figs. 10 and 11, the main differences between compound and heat wave events are the reduced soil moisture and NDVI associated with drought in compound events. The anomalous land surface conditions favor dust emissions. Figure 12 shows density plots of DOD versus soil moisture and NDVI in dust source regions for the whole warm season (March–August), heat wave events, and compound events, respectively. Significant negative relationships are found between DOD and soil moisture and between DOD and NDVI in spring and summer (Figs. 12a,d) and during heat wave events (Figs. 12b,e), consistent with our understanding of dust emission processes; that is, dust is more likely to be lifted to the atmosphere from dry and sparsely vegetated surface. During compound events, the negative connection between DOD and soil moisture becomes weak and nonsignificant, probably because soil moisture is already low during a drought (Fig. 12c). On the other hand, the negative connection between DOD and NDVI is stronger during compound events than heat wave events (Figs. 12e,f), indicating that reduced vegetation coverage plays a primary role in increasing dust emissions in compound events. This is consistent with Pu and Ginoux (2017), who showed that land surface bareness is a dominant local factor affecting dustiness over central to southern California in spring and summer.

What is the circulation pattern associated with California heat wave events, and is it different for compound events? Figure 13 shows the composite of 850- and 500-hPa geopotential height and wind anomalies for heat wave events in nondrought years and the differences in comparison with compound events. An anomalous high is located over the U.S. west coast during heat waves at 850 and 500 hPa, with an anomalous low to the west over the North Pacific around 150°W and a weak high anomaly around 180°W (Figs. 13a,b). Overall, the ridge–trough–ridge pattern resembles the circulation anomaly associated with California Central Valley heat waves (Grotjahn and Faure 2008; Grotjahn 2011; Lee and Grotjahn 2016) and the compound events (Fig. 6).

Brought to you by NOAA Central Library | Unauthenticated | Downloaded 07/19/23 05:08 PM UTC

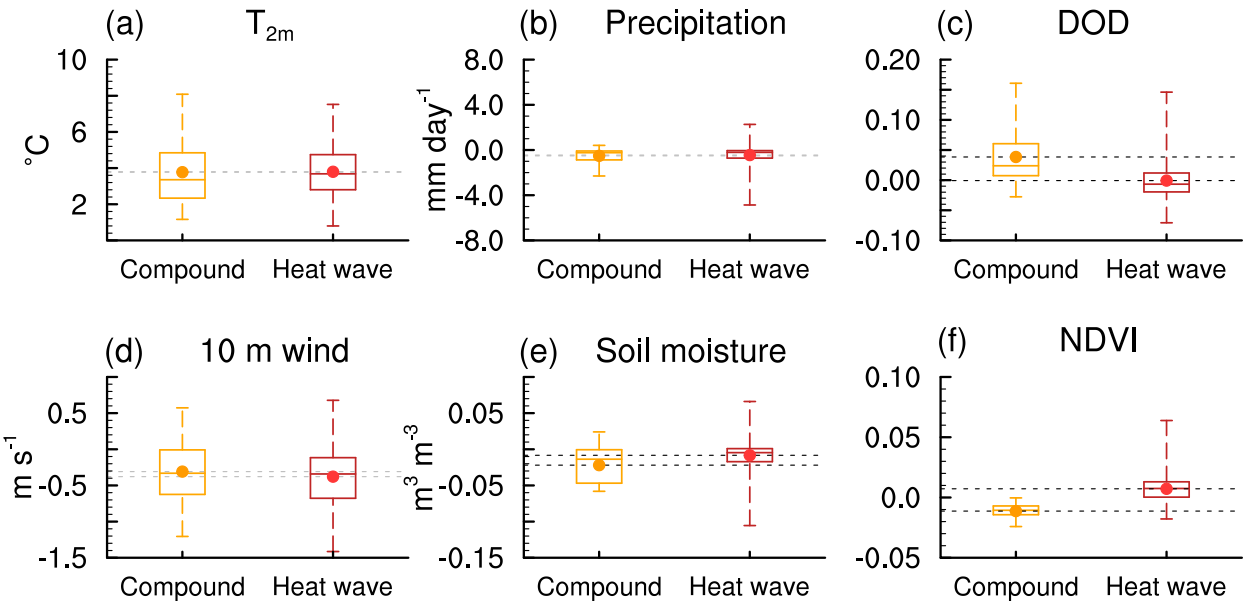

FIG. 11. Boxplots of (a) daily T_{2m} (°C), (b) precipitation (mm day^{-1}), (c) DOD, (d) surface wind speed (m s^{-1}), (e) soil moisture (m^3 m^{-3}), and (f) NDVI anomalies (with reference to the 2003–20 mean) during compound events (orange) and heat wave events (in nondrought years; red). The upper and lower ends of the box correspond to the 25th and 75th percentiles of the data, the bar through the box shows the median, and the dot denotes the mean value. The whiskers extend from the minimum to the maximum of the data. Black or gray dashed lines also mark mean values, with the black lines indicating that the differences of the mean values between compound and heat wave events are significant at the 95% confidence level (*t* test).

The height anomalies over the North Pacific between 130°W–180° and 20°–55°N appear to be stronger in compound events but may be partially due to the greater sample size of heat wave events that can cancel out height anomalies (Figs. 13c,d).

We also compared the features of compound events with all of the heat wave events from 2003 to 2020 (100 events), regardless of whether they are within drought or nondrought years. Greater precipitation and soil moisture deficiency are found in those heat wave composites (Fig. S7 in the online supplemental material). Consistently, weak NDVI reduction and DOD enhancement are found over central to southern California. The differences of soil moisture between compound and heat wave events become smaller and nonsignificant, while the differences in NDVI and DOD remain significant (Fig. S8 in the online supplemental material), indicating that drought induced vegetation decay and consequently increased dustiness is a key feature of compound events. The circulation patterns associated with general heat wave events are very similar to those in nondrought years (Fig. S9 in the online supplemental material).

5. Conclusions

California droughts in the 2000s and 2010s have substantial socioeconomic and environmental impacts. Although high temperature extremes are reported during the 2011–16 California drought (e.g., Seager and Hoerling 2014), little work has been done to examine the concurrent California drought and heat waves. Enhanced dust activities are also found during droughts in the central and southwestern United States (Pu and Ginoux 2017). To the best of our knowledge, compound drought, heat wave, and dusty conditions in California have not been examined. In this work, we examine concurrent drought, heat wave, and dust events in California, so-called compound events, during warm seasons and compare compound events with California heat wave events.

We found 16 compound events in spring and summer during 2003–20, with an average duration of about four days. During these events, California daily maximum temperature increases by about 4.5°C on average, precipitation decreases by about 0.5 mm day^{-1} (~72% of the March–August mean over 2003–20), and dust optical depth increases by about −0.04 (~70% of warm-season mean). The warming is strongest over northern to western California, while precipitation and soil moisture reduction occur largely over northern California and the northern part of central California. Vegetation also declines over central to southern California, which greatly favors the dust emissions by leaving dry land surface unprotected. The anomalous easterly surface winds over large parts of California tend to weaken the cooling sea breeze, which is a well-known pattern during California heat waves. Over central California, the anomalous southeasterly winds favor the northward transport of dust from source regions in the south.

The development of compound events is associated with an anomalous high over the northwest coast of the United States at lower to middle troposphere, which is part of a nearly stationary wave train over the North Pacific. The anomalous high appears over the North Pacific Ocean about 7 days before the compound events and slowly extends eastward. The circulation patterns are similar to that of warm-season California heat

Brought to you by NOAA Central Library | Unauthenticated | Downloaded 07/19/23 05:08 PM UTC

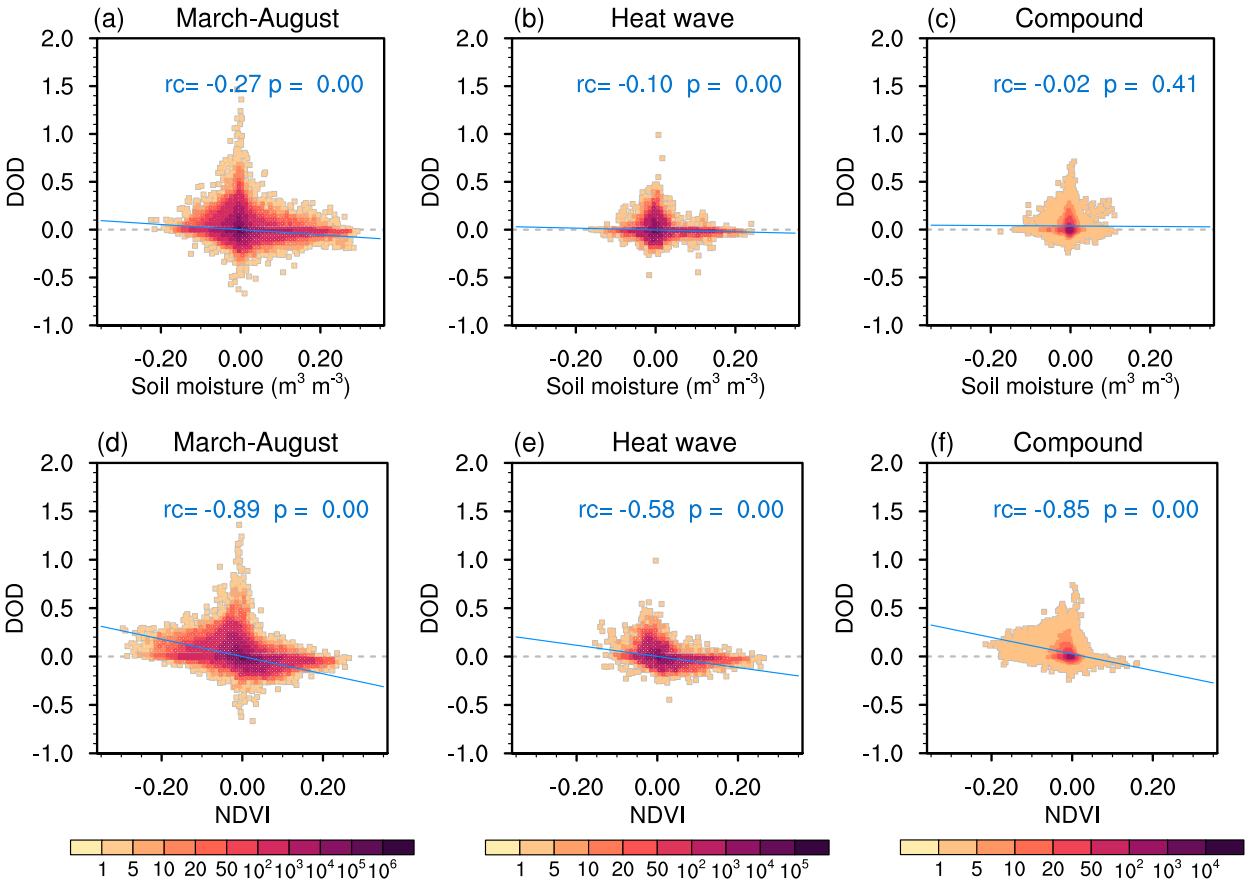

FIG. 12. Density plot of (a)–(c) DOD vs soil moisture and (d)–(f) DOD vs NDVI over dust source regions for (left) March–August, (center) heat wave events (nondrought years), and (right) compound events during 2003–20. All data are interpolated to a 0.1° × 0.1° grid. Shading indicates number of grid boxes within the intervals shown by the *x* and *y* axes. The fitting (blue line) is calculated using the original data without grouping.

waves, although the coastal anomalous high is stronger, and the zonal wavelength of the wave train is slightly longer in compound events. A weak cooling over the western to central tropical Pacific is found to be associated with compound events.

The anomalous atmospheric circulation patterns associated with the compound events (e.g., low surface winds, lack of precipitation, and subsidence inversion associated with the anomalous high) also favor the accumulation of pollutants. Over central to northern California, near-surface fine dust and $PM_{2.5}$ concentrations increase by more than 0.5 and 5 $\mu g\ m^{-3}$, respectively (~70% of their March–August means during 2003–20). In addition to enhanced dust emissions, photochemical reactions under high radiation during heat waves (e.g., Tressol et al. 2008) and enhanced anthropogenic emissions associated with extra energy consumptions during droughts (Christian-Smith et al. 2011; Herrera-Estrada et al. 2018) and heat waves could also contribute to poor air quality in compound events.

Compound events also show unique features different form California heat wave events. While heat waves are generally associated with reduced precipitation and soil moisture, soil moisture reduction during heat waves in nondrought years is significantly weaker than that of compound events. In addition, drought-induced vegetation decay (or reduced NDVI) in compound events is much stronger than heat wave events and promotes dust emissions.

This work for the first time characterizes the features of concurrent drought, heat wave, and dust events in California and examines their development. Compound events occur during droughts; when soil moisture is in deficit and NDVI is low, with favorable atmospheric conditions (i.e., an anomalous high over the U.S. West Coast), California experiences high temperature extremes and enhanced DOD and surface fine dust concentrations, along with degraded air quality. Future studies of variations in compound events, their environmental impacts, and potential interactions with wildfire events will help us better quantify and project their combined negative effects.

Acknowledgments. IMPROVE is a collaborative association of state, tribal, and federal agencies and international partners. The U.S. Environmental Protection Agency is the primary funding source, with contracting and research support from the National Park Service. The Air Quality Group at the University of California, Davis, is the central analytical laboratory, with

Brought to you by NOAA Central Library | Unauthenticated | Downloaded 07/19/23 05:08 PM UTC

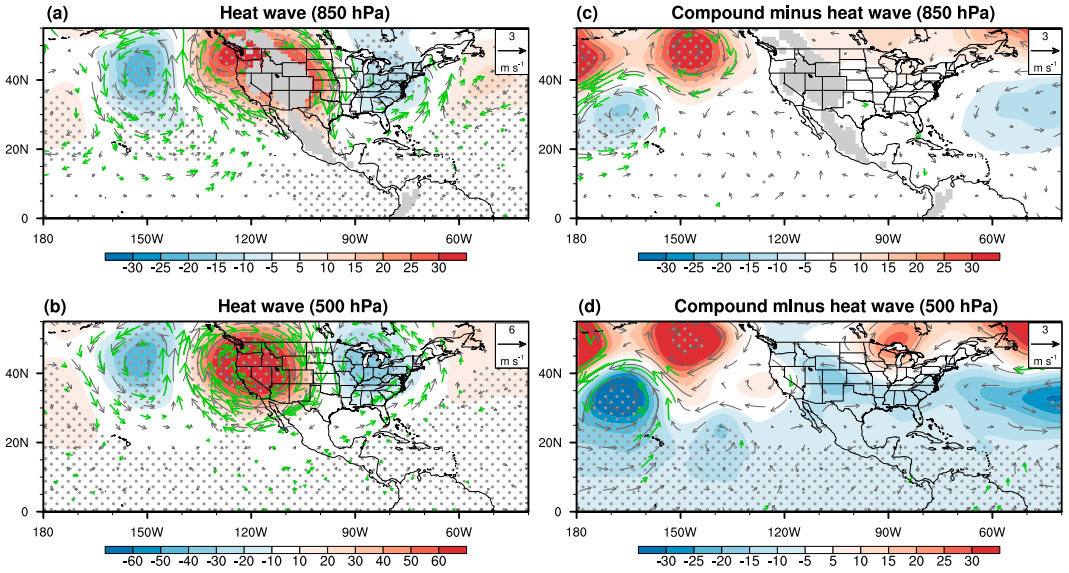

FIG. 13. Composites of (a) 850- and (b) 500-hPa geopotential height (gpm) and wind (m s^{-1}) anomalies (with reference to the 2003–20 mean) during California heat wave events (nondrought years) and (c),(d) the respective differences of 850- and 500-hPa geopotential height and winds between compound and heat wave events. The area significant at the 95% confidence level (*t* test) is stippled. Winds significant at the 95% confidence level are plotted as green vectors. Topography is masked out in gray.

ion analysis provided by Research Triangle Institute and carbon analysis provided by Desert Research Institute. Valuable comments from Dr. John Dunne improved the paper and are sincerely appreciated. The insightful comments from four anonymous reviewers improved the paper.

Data availability statement. The ERA5 reanalysis product is publicly available (https://www.ecmwf.int/en/forecasts/datasets/reanalysis-datasets/era5). CRU and PRECL precipitation data are available at https://crudata.uea.ac.uk/cru/data/hrg/ and https://psl.noaa.gov/data/gridded/data.precl.html, respectively. IMPROVE fine dust data are accessible online (http://views.cira.colostate.edu/fed/DataWizard/), as are EPA AQS data (https://www.epa.gov/aqs). MODIS products are publicly available (https://earthdata.nasa.gov/).

REFERENCES

Achakulwisut, P., L. Shen, and L. J. Mickley, 2017: What controls springtime fine dust variability in the western United States? Investigating the 2002–2015 increase in fine dust in the U.S. Southwest. *J. Geophys. Res. Atmos.*, **122**, 12 449–12 467, https://doi.org/10.1002/2017JD027208.

AghaKouchak, A., L. Y. Cheng, O. Mazdiyasni, and A. Farahmand, 2014: Global warming and changes in risk of concurrent climate extremes: Insights from the 2014 California drought. *Geophys. Res. Lett.*, **41**, 8847–8852, https://doi.org/10.1002/2014GL062308.

Awasthi, A., K. Vishwakarma, and K. C. Pattnayak, 2022: Retrospection of heatwave and heat index. *Theor. Appl. Climatol.*, **147**, 589–604, https://doi.org/10.1007/s00704-021-03854-z.

Baddock, M. C., P. Ginoux, J. E. Bullard, and T. E. Gill, 2016: Do MODIS-defined dust sources have a geomorphological signature? *Geophys. Res. Lett.*, **43**, 2606–2613, https://doi.org/10.1002/2015GL067327.

Bao, J. W., S. A. Michelson, P. O. G. Persson, I. V. Djalalova, and J. M. Wilczak, 2008: Observed and WRF-simulated low-level winds in a high-ozone episode during the Central California Ozone Study. *J. Appl. Meteor. Climatol.*, **47**, 2372–2394, https://doi.org/10.1175/2008JAMC1822.1.

Beck, H. E., and Coauthors, 2021: Evaluation of 18 satellite- and model-based soil moisture products using in situ measurements from 826 sensors. *Hydrol. Earth Syst. Sci.*, **25**, 17–40, https://doi.org/10.5194/hess-25-17-2021.

Bilby, T., L. Baumgard, R. Collier, R. Zimbelman, and M. Rhoads, 2008: Heat stress effects on fertility: Consequences and possible solutions. *Proc. Southwest Nutrition Conf.,* Tempe, AZ, University of Arizona, 177–193.

Borlina, C. S., and N. O. Rennó, 2017: The impact of a severe drought on dust lifting in California's Owens Lake area. *Sci. Rep.*, **7**, 1784, https://doi.org/10.1038/s41598-017-01829-7.

Brown, J. F., and M. S. Pervez, 2014: Merging remote sensing data and national agricultural statistics to model change in irrigated agriculture. *Agric. Syst.*, **127**, 28–40, https://doi.org/10.1016/j.agsy.2014.01.004.

Chen, M. Y., P. P. Xie, J. E. Janowiak, and P. A. Arkin, 2002: Global land precipitation: A 50-yr monthly analysis based on gauge observations. *J. Hydrometeor.*, **3**, 249–266, https://doi.org/10.1175/1525-7541(2002)003<0249:GLPAYM>2.0.CO;2.

Chow, J. C., J. G. Watson, D. H. Lowenthal, P. A. Solomon, K. L. Magliano, S. D. Ziman, and L. W. Richards, 1992: PM10 source apportionment in California's San Joaquin Valley. *Atmos. Environ.*, **26A,** 3335–3354, https://doi.org/10.1016/0960-1686(92)90350-T.

——, ——, L. L. Ashbaugh, and K. L. Magliano, 2003: Similarities and differences in PM10 chemical source profiles for geological dust from the San Joaquin Valley, California.

Brought to you by NOAA Central Library | Unauthenticated | Downloaded 07/19/23 05:08 PM UTC

Atmos. Environ., **37**, 1317–1340, https://doi.org/10.1016/S1352-2310(02)01021-X.

Christian-Smith, J., M. Levy, and P. H. Gleick, 2011: Impacts of the California drought from 2007 to 2009. Pacific Institute Rep., 105 pp., https://pacinst.org/wp-content/uploads/2011/06/ca_drought_impacts_full_report3.pdf.

Clausnitzer, H., and M. J. Singer, 1996: Respirable-dust production from agricultural operations in the Sacramento Valley, California. *J. Environ. Qual.*, **25**, 877–884, https://doi.org/10.2134/jeq1996.00472425002500040032x.

Clemesha, R. E. S., K. Guirguis, A. Gershunov, I. J. Small, and A. Tardy, 2018: California heat waves: Their spatial evolution, variation, and coastal modulation by low clouds. *Climate Dyn.*, **50**, 4285–4301, https://doi.org/10.1007/s00382-017-3875-7.

Conil, S., and A. Hall, 2006: Local regimes of atmospheric variability: A case study of southern California. *J. Climate*, **19**, 4308–4325, https://doi.org/10.1175/JCLI3837.1.

Cook, B. I., R. L. Miller, and R. Seager, 2009: Amplification of the North American "Dust Bowl" drought through human-induced land degradation. *Proc. Natl. Acad. Sci. USA*, **106**, 4997–5001, https://doi.org/10.1073/pnas.0810200106.

——, T. R. Ault, and J. E. Smerdon, 2015: Unprecedented 21st century drought risk in the American Southwest and Central Plains. *Sci. Adv.*, **1**, e1400082, https://doi.org/10.1126/sciadv.1400082.

Creamean, J. M., J. R. Spackman, S. M. Davis, and A. B. White, 2014: Climatology of long-range transported Asian dust along the West Coast of the United States. *J. Geophys. Res. Atmos.*, **119**, 12 171–12 185, https://doi.org/10.1002/2014JD021694.

Crooks, J. L., W. E. Cascio, M. S. Percy, J. Reyes, L. M. Neas, and E. D. Hilborn, 2016: The association between dust storms and daily non-accidental mortality in the United States, 1993–2005. *Environ. Health Perspect.*, **124**, 1735–1743, https://doi.org/10.1289/EHP216.

Cui, W. J., X. Q. Dong, B. K. Xi, Z. Feng, and J. W. Fan, 2020: Can the GPM IMERG final product accurately represent MCSs' precipitation characteristics over the central and eastern United States? *J. Hydrometeor.*, **21**, 39–57, https://doi.org/10.1175/JHM-D-19-0123.1.

Dezfuli, A. K., C. M. Ichoku, G. J. Huffman, K. I. Mohr, J. S. Selker, N. van de Giesen, R. Hochreutener, and F. O. Annor, 2017: Validation of IMERG precipitation in Africa. *J. Hydrometeor.*, **18**, 2817–2825, https://doi.org/10.1175/JHM-D-17-0139.1.

Didan, K., 2015a: MOD13C1 MODIS/*Terra* vegetation indices 16-day L3 global 0.05deg CMG V006. NASA EOSDIS Land Processes DAAC, accessed 2 September 2021, https://doi.org/10.5067/MODIS/MOD13C1.006.

——, 2015b: MOD13C2 MODIS/*Terra* vegetation indices monthly L3 global 0.05deg CMG V006. NASA EOSDIS Land Processes DAAC, accessed xxxx, https://doi.org/10.5067/MODIS/MOD13C2.006.

Diffenbaugh, N. S., D. L. Swain, and D. Touma, 2015: Anthropogenic warming has increased drought risk in California. *Proc. Natl. Acad. Sci. USA*, **112**, 3931–3936, https://doi.org/10.1073/pnas.1422385112.

Dirmeyer, P. A., G. Balsamo, E. M. Blyth, R. Morrison, and H. M. Cooper, 2021: Land–atmosphere interactions exacerbated the drought and heatwave over Northern Europe during summer 2018. *AGU Adv.*, **2**, e2020AV000283, https://doi.org/10.1029/2020AV000283.

Dukes, D., H. B. Gonzales, S. Ravi, D. E. Grandstaff, R. S. Van Pelt, J. R. Li, G. Wang, and J. B. Sankey, 2018: Quantifying postfire aeolian sediment transport using rare earth element tracers. *J. Geophys. Res. Biogeosci.*, **123**, 288–299, https://doi.org/10.1002/2017JG004284.

Fécan, F., B. Marticorena, and G. Bergametti, 1999: Parametrization of the increase of the aeolian erosion threshold wind friction velocity due to soil moisture for arid and semi-arid areas. *Ann. Geophys.*, **17**, 149–157, https://doi.org/10.1007/s00585-999-0149-7.

Fischer, E. V., N. C. Hsu, D. A. Jaffe, M. J. Jeong, and S. L. Gong, 2009: A decade of dust: Asian dust and springtime aerosol load in the US Pacific Northwest. *Geophys. Res. Lett.*, **36**, L03821, https://doi.org/10.1029/2008GL036467.

Freychet, N., G. Hegerl, D. Mitchell, and M. Collins, 2021: Future changes in the frequency of temperature extremes may be underestimated in tropical and subtropical regions. *Commun. Earth Environ.*, **2**, 28, https://doi.org/10.1038/s43247-021-00094-x.

Gaudichet, A., and Coauthors, 1995: Trace-elements in tropical African savanna biomass burning aerosols. *J. Atmos. Chem.*, **22**, 19–39, https://doi.org/10.1007/BF00708179.

Gelaro, R., and Coauthors, 2017: The Modern-Era Retrospective Analysis for Research and Applications, version 2 (MERRA-2). *J. Climate*, **30**, 5419–5454, https://doi.org/10.1175/JCLI-D-16-0758.1.

Gershunov, A., and K. Guirguis, 2012: California heat waves in the present and future. *Geophys. Res. Lett.*, **39**, L18710, https://doi.org/10.1029/2012GL052979.

——, D. R. Cayan, and S. F. Iacobellis, 2009: The great 2006 heat wave over California and Nevada: Signal of an increasing trend. *J. Climate*, **22**, 6181–6203, https://doi.org/10.1175/2009JCLI2465.1.

Gill, T. E., 1996: Eolian sediments generated by anthropogenic disturbance of playas: Human impacts on the geomorphic system and geomorphic impacts on the human system. *Geomorphology*, **17**, 207–228, https://doi.org/10.1016/0169-555X(95)00104-D.

Gillette, D. A., and R. Passi, 1988: Modeling dust emission caused by wind erosion. *J. Geophys. Res.*, **93**, 14 233–14 242, https://doi.org/10.1029/JD093iD11p14233.

Ginoux, P., D. Garbuzov, and N. C. Hsu, 2010: Identification of anthropogenic and natural dust sources using Moderate Resolution Imaging Spectroradiometer (MODIS) Deep Blue level 2 data. *J. Geophys. Res.*, **115**, D05204, https://doi.org/10.1029/2009JD012398.

——, J. M. Prospero, T. E. Gill, N. C. Hsu, and M. Zhao, 2012: Global-scale attribution of anthropogenic and natural dust sources and their emission rates based on MODIS deep blue aerosol products. *Rev. Geophys.*, **50**, RG3005, https://doi.org/10.1029/2012RG000388.

Goldewijk, K. K., A. Beusen, J. Doelman, and E. Stehfest, 2017: Anthropogenic land use estimates for the Holocene—HYDE 3.2. *Earth Syst. Sci. Data*, **9**, 927–953, https://doi.org/10.5194/essd-9-927-2017.

Goudie, A. S., 2009: Dust storms: Recent developments. *J. Environ. Manage.*, **90**, 89–94, https://doi.org/10.1016/j.jenvman.2008.07.007.

Gouveia, C. M., J. P. A. Martins, A. Russo, R. Durao, and I. F. Trigo, 2022: Monitoring heat extremes across central Europe using land surface temperature data records from SEVIRI/MSG. *Remote Sens.*, **14**, 3470, https://doi.org/10.3390/rs14143470.

Grotjahn, R., 2011: Identifying extreme hottest days from large scale upper air data: A pilot scheme to find California Central Valley summertime maximum surface temperatures. *Climate Dyn.*, **37**, 587–604, https://doi.org/10.1007/s00382-011-0999-z.

——, and G. Faure, 2008: Composite predictor maps of extraordinary weather events in the Sacramento, California, region. *Wea. Forecasting*, **23**, 313–335, https://doi.org/10.1175/2007WAF2006055.1.

Brought to you by NOAA Central Library | Unauthenticated | Downloaded 07/19/23 05:08 PM UTC

——, and Y. Y. Lee, 2016: On climate model simulations of the large-scale meteorology associated with California heat waves. *J. Geophys. Res. Atmos.*, **121**, 18–32, https://doi.org/10.1002/2015JD024191.

——, and Coauthors, 2016: North American extreme temperature events and related large scale meteorological patterns: A review of statistical methods, dynamics, modeling, and trends. *Climate Dyn.*, **46**, 1151–1184, https://doi.org/10.1007/s00382-015-2638-6.

Hand, J. L., and Coauthors, 2011: Spatial and seasonal patterns and temporal variability of haze and its constituents in the United States. IMPROVE Rep. V, 507 pp., http://vista.cira.colostate.edu/Improve/spatial-and-seasonal-patterns-and-temporal-variability-of-haze-and-its-constituents-in-the-united-states-report-v-june-2011/.

——, T. E. Gill, and B. A. Schichtel, 2017: Spatial and seasonal variability in fine mineral dust and coarse aerosol mass at remote sites across the United States. *J. Geophys. Res. Atmos.*, **122**, 3080–3097, https://doi.org/10.1002/2016JD026290.

Harris, I. C., and P. D. Jones, 2020: CRU TS4.03: Climatic Research Unit (CRU) Time-Series (TS) version 4.03 of high-resolution gridded data of month-by-month variation in climate (Jan. 1901–Dec. 2018). Centre for Environmental Data Analysis, accessed 22 January 2020, https://doi.org/10.5285/10d3e3640f004c578403419aac167d82.

Herrera-Estrada, J. E., N. S. Diffenbaugh, F. Wagner, A. Craft, and J. Sheffield, 2018: Response of electricity sector air pollution emissions to drought conditions in the western United States. *Environ. Res. Lett.*, **13**, 124032, https://doi.org/10.1088/1748-9326/aaf07b.

Hersbach, H., and Coauthors, 2020: The ERA5 global reanalysis. *Quart. J. Roy. Meteor. Soc.*, **146**, 1999–2049, https://doi.org/10.1002/qj.3803.

Hirschi, M., and Coauthors, 2011: Observational evidence for soil-moisture impact on hot extremes in southeastern Europe. *Nat. Geosci.*, **4**, 17–21, https://doi.org/10.1038/ngeo1032.

Hoerling, M., J. Eischeid, and J. Perlwitz, 2010: Regional precipitation trends: Distinguishing natural variability from anthropogenic forcing. *J. Climate*, **23**, 2131–2145, https://doi.org/10.1175/2009JCLI3420.1.

Horton, R. M., J. S. Mankin, C. Lesk, E. Coffel, and C. Raymond, 2016: A review of recent advances in research on extreme heat events. *Curr. Climate Change Rep.*, **2**, 242–259, https://doi.org/10.1007/s40641-016-0042-x.

Huete, A., C. O. Justice, and W. van Leeuwen, 1999: MODIS vegetation index (MOD13) algorithm theoretical basis document: version 3. University of Virginia Dept. of Environmental Sciences Doc., 120 pp., https://modis.gsfc.nasa.gov/data/atbd/atbd_mod13.pdf.

Huffman, G. J., and Coauthors, 2019: NASA Global Precipitation Measurement (GPM) Integrated Multi-satellitE Retrievals for GPM (IMERG). NASA Goddard Space Flight Center Algorithm Theoretical Basis Doc. (ATBD), version 5.2, 31 pp., https://gpm.nasa.gov/sites/default/files/document_files/IMERG_ATBD_V5.2_0.pdf.

Hughes, M., and A. Hall, 2010: Local and synoptic mechanisms causing Southern California's Santa Ana winds. *Climate Dyn.*, **34**, 847–857, https://doi.org/10.1007/s00382-009-0650-4.

Jaeger, E. B., and S. I. Seneviratne, 2011: Impact of soil moisture–atmosphere coupling on European climate extremes and trends in a regional climate model. *Climate Dyn.*, **36**, 1919–1939, https://doi.org/10.1007/s00382-010-0780-8.

Jin, Q. J., J. F. Wei, W. K. M. Lau, B. Pu, and C. Wang, 2021: Interactions of Asian mineral dust with Indian summer monsoon: Recent advances and challenges. *Earth-Sci. Rev.*, **215**, 103562, https://doi.org/10.1016/j.earscirev.2021.103562.

Kavouras, I. G., G. Nikolich, V. Etyemezian, D. W. DuBois, J. King, and D. Shafer, 2012: In situ observations of soil minerals and organic matter in the early phases of prescribed fires. *J. Geophys. Res.*, **117**, D12313, https://doi.org/10.1029/2011JD017420.

Knowlton, K., M. Rotkin-Ellman, G. King, H. G. Margolis, D. Smith, G. Solomon, R. Trent, and P. English, 2009: The 2006 California heat wave: Impacts on hospitalizations and emergency department visits. *Environ. Health Perspect.*, **117**, 61–67, https://doi.org/10.1289/ehp.11594.

Kok, J. F., and Coauthors, 2021: Contribution of the world's main dust source regions to the global cycle of desert dust. *Atmos. Chem. Phys.*, **21**, 8169–8193, https://doi.org/10.5194/acp-21-8169-2021.

Kolivras, K. N., and A. C. Comrie, 2004: Climate and infectious disease in the southwestern United States. *Prog. Phys. Geogr.*, **28**, 387–398, https://doi.org/10.1191/0309133304pp417ra.

Lau, N. C., and M. J. Nath, 2012: A model study of heat waves over North America: Meteorological aspects and projections for the twenty-first century. *J. Climate*, **25**, 4761–4784, https://doi.org/10.1175/JCLI-D-11-00575.1.

Lee, Y. Y., and R. Grotjahn, 2016: California Central Valley summer heat waves form two ways. *J. Climate*, **29**, 1201–1217, https://doi.org/10.1175/JCLI-D-15-0270.1.

——, and ——, 2019: Evidence of specific MJO phase occurrence with summertime California central valley extreme hot weather. *Adv. Atmos. Sci.*, **36**, 589–602, https://doi.org/10.1007/s00376-019-8167-1.

Li, M. X., P. L. Wu, and Z. G. Ma, 2020: A comprehensive evaluation of soil moisture and soil temperature from third-generation atmospheric and land reanalysis data sets. *Int. J. Climatol.*, **40**, 5744–5766, https://doi.org/10.1002/joc.6549.

Li, Z., G. Q. Tang, P. Kirstetter, S. Gao, J. L. F. Li, Y. X. Wen, and Y. Hong, 2022: Evaluation of GPM IMERG and its constellations in extreme events over the conterminous United States. *J. Hydrol.*, **606**, 127357, https://doi.org/10.1016/j.jhydrol.2021.127357.

Lund, J., J. Medellin-Azuara, J. Durand, and K. Stone, 2018: Lessons from California's 2012–2016 drought. *J. Water Res. Plann. Manage.*, **144** (10), 1–13, https://doi.org/10.1061/(ASCE)WR.1943-5452.0000984.

Maenhaut, W., I. Salma, J. Cafmeyer, H. J. Annegarn, and M. O. Andreae, 1996: Regional atmospheric aerosol composition and sources in the eastern Transvaal, South Africa, and impact of biomass burning. *J. Geophys. Res.*, **101**, 23 631–23 650, https://doi.org/10.1029/95JD02930.

Malm, W. C., J. F. Sisler, D. Huffman, R. A. Eldred, and T. A. Cahill, 1994: Spatial and seasonal trends in particle concentration and optical extinction in the United States. *J. Geophys. Res.*, **99**, 1347–1370, https://doi.org/10.1029/93JD02916.

Mazdiyasni, O., and A. AghaKouchak, 2015: Substantial increase in concurrent droughts and heatwaves in the United States. *Proc. Natl. Acad. Sci. USA*, **112**, 11 484–11 489, https://doi.org/10.1073/pnas.1422945112.

Merino-Martín, L., J. P. Field, J. C. Villegas, J. J. Whicker, D. D. Breshears, D. J. Law, and A. M. Urgeghe, 2014: Aeolian sediment and dust fluxes during predominant "background" wind conditions for unburned and burned semiarid grassland: Interplay between particle size and temporal scale. *Aeolian Res.*, **14**, 97–103, https://doi.org/10.1016/j.aeolia.2014.02.004.

Brought to you by NOAA Central Library | Unauthenticated | Downloaded 07/19/23 05:08 PM UTC

Mueller, B., and S. I. Seneviratne, 2012: Hot days induced by precipitation deficits at the global scale. *Proc. Natl. Acad. Sci. USA*, **109**, 12 398–12 403, https://doi.org/10.1073/pnas.1204330109.

Nisantzi, A., R. E. Mamouri, A. Ansmann, and D. Hadjimitsis, 2014: Injection of mineral dust into the free troposphere during fire events observed with polarization lidar at Limassol, Cyprus. *Atmos. Chem. Phys.*, **14**, 12 155–12 165, https://doi.org/10.5194/acp-14-12155-2014.

Painter, T. H., J. S. Deems, J. Belnap, A. F. Hamlet, C. C. Landry, and B. Udall, 2010: Response of Colorado River runoff to dust radiative forcing in snow. *Proc. Natl. Acad. Sci. USA*, **107**, 17 125–17 130, https://doi.org/10.1073/pnas.0913139107.

Palipane, E., and R. Grotjahn, 2018: Future projections of the large-scale meteorology associated with California heat waves in CMIP5 models. *J. Geophys. Res. Atmos.*, **123**, 8500–8517, https://doi.org/10.1029/2018JD029000.

Perkins, S. E., 2015: A review on the scientific understanding of heatwaves—Their measurement, driving mechanisms, and changes at the global scale. *Atmos. Res.*, **164–165**, 242–267, https://doi.org/10.1016/j.atmosres.2015.05.014.

——, and L. V. Alexander, 2013: On the measurement of heat waves. *J. Climate*, **26**, 4500–4517, https://doi.org/10.1175/JCLI-D-12-00383.1.

——, ——, and J. R. Nairn, 2012: Increasing frequency, intensity and duration of observed global heatwaves and warm spells. *Geophys. Res. Lett.*, **39**, L20714, https://doi.org/10.1029/2012GL053361.

Pervez, M. S., and J. F. Brown, 2010: Mapping irrigated lands at 250-m scale by merging MODIS data and national agricultural statistics. *Remote Sens.*, **2**, 2388–2412, https://doi.org/10.3390/rs2102388.

Prospero, J. M., P. Ginoux, O. Torres, S. E. Nicholson, and T. E. Gill, 2002: Environmental characterization of global sources of atmospheric soil dust identified with the *Nimbus 7* Total Ozone Mapping Spectrometer (TOMS) absorbing aerosol product. *Rev. Geophys.*, **40**, 1002, https://doi.org/10.1029/2000RG000095.

Pu, B., and P. Ginoux, 2016: The impact of the Pacific Decadal Oscillation on springtime dust activity in Syria. *Atmos. Chem. Phys.*, **16**, 13 431–13 448, https://doi.org/10.5194/acp-16-13431-2016.

——, and ——, 2017: Projection of American dustiness in the late 21st century due to climate change. *Sci. Rep.*, **7**, 5553, https://doi.org/10.1038/s41598-017-05431-9.

——, and ——, 2018a: Climatic factors contributing to long-term variations in surface fine dust concentration in the United States. *Atmos. Chem. Phys.*, **18**, 4201–4215, https://doi.org/10.5194/acp-18-4201-2018.

——, and ——, 2018b: How reliable are CMIP5 models in simulating dust optical depth? *Atmos. Chem. Phys.*, **18**, 12 491–12 510, https://doi.org/10.5194/acp-18-12491-2018.

——, and Q. J. Jin, 2021: A record-breaking trans-Atlantic African dust plume associated with atmospheric circulation extremes in June 2020. *Bull. Amer. Meteor. Soc.*, **102**, E1340–E1356, https://doi.org/10.1175/BAMS-D-21-0014.1.

Raphael, M. N., 2003: The Santa Ana winds of California. *Earth Interact.*, **7**, https://doi.org./10.1175/1087-3562(2003)007<0001:TSAWOC>2.0.CO;2.

Raupach, M. R., 1994: Simplified expressions for vegetation roughness length and zero-plane displacement as functions of canopy height and area index. *Bound.-Layer Meteor.*, **71**, 211–216, https://doi.org/10.1007/BF00709229.

Ravi, S., P. D'Odorico, T. M. Zobeck, T. M. Over, and S. L. Collins, 2007: Feedbacks between fires and wind erosion in heterogeneous arid lands. *J. Geophys. Res.*, **112**, G04007, https://doi.org/10.1029/2007JG000474.

——, M. C. Baddock, T. M. Zobeck, and J. Hartman, 2012: Field evidence for differences in post-fire Aeolian transport related to vegetation type in semi-arid grasslands. *Aeolian Res.*, **7**, 3–10, https://doi.org/10.1016/j.aeolia.2011.12.002.

Rogers, C. D. W., K. Kornhuber, S. E. Perkins-Kirkpatrick, P. C. Loikith, and D. Singh, 2022: Sixfold increase in historical Northern Hemisphere concurrent large heatwaves driven by warming and changing atmospheric circulations. *J. Climate*, **35**, 1063–1078, https://doi.org/10.1175/JCLI-D-21-0200.1.

Sayer, A. M., N. C. Hsu, J. Lee, W. V. Kim, and S. T. Dutcher, 2019: Validation, stability, and consistency of MODIS collection 6.1 and VIIRS version 1 Deep Blue aerosol data over land. *J. Geophys. Res. Atmos.*, **124**, 4658–4688, https://doi.org/10.1029/2018JD029598.

Schepanski, K., I. Tegen, and A. Macke, 2012: Comparison of satellite based observations of Saharan dust source areas. *Remote Sens. Environ.*, **123**, 90–97, https://doi.org/10.1016/j.rse.2012.03.019.

Schlosser, J. S., and Coauthors, 2017: Analysis of aerosol composition data for western United States wildfires between 2005 and 2015: Dust emissions, chloride depletion, and most enhanced aerosol constituents. *J. Geophys. Res. Atmos.*, **122**, 8951–8966, https://doi.org/10.1002/2017JD026547.

Schubert, S. D., H. L. Wang, R. D. Koster, M. J. Suarez, and P. Ya. Groisman, 2014: Northern Eurasian heat waves and droughts. *J. Climate*, **27**, 3169–3207, https://doi.org/10.1175/JCLI-D-13-00360.1.

Schweitzer, M. D., A. S. Calzadilla, O. Salamo, A. Sharifi, N. Kumar, G. Holt, M. Campos, and M. Mirsaeidi, 2018: Lung health in era of climate change and dust storms. *Environ. Res.*, **163**, 36–42, https://doi.org/10.1016/j.envres.2018.02.001.

Seager, R., 2007: The turn of the century North American drought: Global context, dynamics, and past analogs. *J. Climate*, **20**, 5527–5552, https://doi.org/10.1175/2007JCLI1529.1.

——, and G. A. Vecchi, 2010: Greenhouse warming and the 21st century hydroclimate of southwestern North America. *Proc. Natl. Acad. Sci. USA*, **107**, 21 277–21 282, https://doi.org/10.1073/pnas.0910856107.

——, and M. Hoerling, 2014: Atmosphere and ocean origins of North American droughts. *J. Climate*, **27**, 4581–4606, https://doi.org/10.1175/JCLI-D-13-00329.1.

——, ——, S. Schubert, H. L. Wang, B. Lyon, A. Kumar, J. Nakamura, and N. Henderson, 2015: Causes of the 2011–14 California drought. *J. Climate*, **28**, 6997–7024, https://doi.org/10.1175/JCLI-D-14-00860.1.

Shukla, S., M. Safeeq, A. AghaKouchak, K. Guan, and C. Funk, 2015: Temperature impacts on the water year 2014 drought in California. *Geophys. Res. Lett.*, **42**, 4384–4393, https://doi.org/10.1002/2015GL063666.

Sungmin, O., and P. E. Kirstetter, 2018: Evaluation of diurnal variation of GPM IMERG-derived summer precipitation over the contiguous US using MRMS data. *Quart. J. Roy. Meteor. Soc.*, **144**, 270–281, https://doi.org/10.1002/qj.3218.

Tan, J., W. A. Petersen, and A. Tokay, 2016: A novel approach to identify sources of errors in IMERG for GPM ground validation. *J. Hydrometeor.*, **17**, 2477–2491, https://doi.org/10.1175/JHM-D-16-0079.1.

——, ——, P. E. Kirstetter, and Y. D. Tian, 2017: Performance of IMERG as a function of spatiotemporal scale. *J. Hydrometeor.*, **18**, 307–319, https://doi.org/10.1175/JHM-D-16-0174.1.

Brought to you by NOAA Central Library | Unauthenticated | Downloaded 07/19/23 05:08 PM UTC

Thompson, V., and Coauthors, 2022: The 2021 western North America heat wave among the most extreme events ever recorded globally. *Sci. Adv.*, **8**, eabm6860, https://doi.org/10.1126/sciadv.abm6860.

Tong, D. Q., J. X. L. Wang, T. E. Gill, H. Lei, and B. Y. Wang, 2017: Intensified dust storm activity and Valley fever infection in the southwestern United States. *Geophys. Res. Lett.*, **44**, 4304–4312, https://doi.org/10.1002/2017GL073524.

Trenberth, K. E., A. G. Dai, G. van der Schrier, P. D. Jones, J. Barichivich, K. R. Briffa, and J. Sheffield, 2014: Global warming and changes in drought. *Nat. Climate Change*, **4**, 17–22, https://doi.org/10.1038/nclimate2067.

Tressol, M., and Coauthors, 2008: Air pollution during the 2003 European heat wave as seen by MOZAIC airliners. *Atmos. Chem. Phys.*, **8**, 2133–2150, https://doi.org/10.5194/acp-8-2133-2008.

Ullrich, P. A., Z. Xu, A. M. Rhoades, M. D. Dettinger, J. F. Mount, A. D. Jones, and P. Vahmani, 2018: California's drought of the future: A midcentury recreation of the exceptional conditions of 2012–2017. *Earth's Future*, **6**, 1568–1587, https://doi.org/10.1029/2018EF001007.

VanCuren, R. A., and T. A. Cahill, 2002: Asian aerosols in North America: Frequency and concentration of fine dust. *J. Geophys. Res.*, **107**, 4804, https://doi.org/10.1029/2002JD002204.

Vukovic, A., and Coauthors, 2014: Numerical simulation of "an American haboob." *Atmos. Chem. Phys.*, **14**, 3211–3230, https://doi.org/10.5194/acp-14-3211-2014.

Wagenbrenner, N. S., M. J. Germino, B. K. Lamb, P. R. Robichaud, and R. B. Foltz, 2013: Wind erosion from a sagebrush steppe burned by wildfire: Measurements of PM10 and total horizontal sediment flux. *Aeolian Res.*, **10**, 25–36, https://doi.org/10.1016/j.aeolia.2012.10.003.

——, S. H. Chung, and B. K. Lamb, 2017: A large source of dust missing in particulate matter emission inventories? Wind erosion of post-fire landscapes. *Elem. Sci. Anthrop.*, **5**, 2, https://doi.org/10.1525/elementa.185.

Wagner, R., M. Jahn, and K. Schepanski, 2018: Wildfires as a source of airborne mineral dust—Revisiting a conceptual model using large-eddy simulation (LES). *Atmos. Chem. Phys.*, **18**, 11 863–11 884, https://doi.org/10.5194/acp-18-11863-2018.

——, K. Schepanski, and M. Klose, 2021: The dust emission potential of agricultural-like fires—Theoretical estimates from two conceptually different dust emission parameterizations. *J. Geophys. Res. Atmos.*, **126**, e2020JD034355, https://doi.org/10.1029/2020JD034355.

Wang, B., and X. S. Xie, 1997: A model for the boreal summer intraseasonal oscillation. *J. Atmos. Sci.*, **54**, 72–86, https://doi.org/10.1175/1520-0469(1997)054<0072:AMFTBS>2.0.CO;2.

Wang, J. X., W. A. Petersen, and D. B. Wolff, 2021: Validation of satellite-based precipitation products from TRMM to GPM. *Remote Sens.*, **13**, 1745, https://doi.org/10.3390/rs13091745.

Weiss, J. L., C. L. Castro, and J. T. Overpeck, 2009: Distinguishing pronounced droughts in the southwestern United States: Seasonality and effects of warmer temperatures. *J. Climate*, **22**, 5918–5932, https://doi.org/10.1175/2009JCLI2905.1.

Wen, Y. X., A. Behrangi, H. N. Chen, and B. Lambrigtsen, 2018: How well were the early 2017 California atmospheric river precipitation events captured by satellite products and ground-based radars? *Quart. J. Roy. Meteor. Soc.*, **144**, 344–359, https://doi.org/10.1002/qj.3253.

Westerling, A. L., D. R. Cayan, T. J. Brown, B. L. Hall, and L. G. Riddle, 2004: Climate, Santa Ana winds and autumn wildfires in southern California. *Eos, Trans. Amer. Geophys. Union*, **85**, 289–300, https://doi.org/10.1029/2004EO310001.

Whicker, J. J., J. E. Pinder, and D. D. Breshears, 2006: Increased wind erosion from forest wildfire: Implications for contaminant-related risks. *J. Environ. Qual.*, **35**, 468–478, https://doi.org/10.2134/jeq2005.0112.

Xiao, M., and Coauthors, 2017: How much groundwater did California's Central Valley lose during the 2012–2016 drought? *Geophys. Res. Lett.*, **44**, 4872–4879, https://doi.org/10.1002/2017GL073333.

Xu, R., F. Q. Tian, L. Yang, H. C. Hu, H. Lu, and A. Z. Hou, 2017: Ground validation of GPM IMERG and TRMM 3B42V7 rainfall products over southern Tibetan Plateau based on a high-density rain gauge network. *J. Geophys. Res. Atmos.*, **122**, 910–924, https://doi.org/10.1002/2016JD025418.

Yang, Y., Z. W. Zhu, T. Li, and M. Y. Yao, 2020: Effects of western Pacific intraseasonal convection on surface air temperature anomalies over North America. *Int. J. Climatol.*, **40**, 2913–2923, https://doi.org/10.1002/joc.6373.

Yu, H. B., L. A. Remer, M. Chin, H. S. Bian, Q. Tan, T. L. Yuan, and Y. Zhang, 2012: Aerosols from overseas rival domestic emissions over North America. *Science*, **337**, 566–569, https://doi.org/10.1126/science.1217576.

Yu, Y., and P. Ginoux, 2021: Assessing the contribution of the ENSO and MJO to Australian dust activity based on satellite- and ground-based observations. *Atmos. Chem. Phys.*, **21**, 8511–8530, https://doi.org/10.5194/acp-21-8511-2021.

——, and ——, 2022: Enhanced dust emission following large wildfires due to vegetation disturbance. *Nat. Geosci.*, **15**, 878–884, https://doi.org/10.1038/s41561-022-01046-6.

——, O. V. Kalashnikova, M. J. Garay, and M. Notaro, 2019: Climatology of Asian dust activation and transport potential based on MISR satellite observations and trajectory analysis. *Atmos. Chem. Phys.*, **19**, 363–378, https://doi.org/10.5194/acp-19-363-2019.

Zaitchik, B. F., A. K. Macalady, L. R. Bonneau, and R. B. Smith, 2006: Europe's 2003 heat wave: A satellite view of impacts and land–atmosphere feedbacks. *Int. J. Climatol.*, **26**, 743–769, https://doi.org/10.1002/joc.1280.

Zender, C. S., and E. Y. Kwon, 2005: Regional contrasts in dust emission responses to climate. *J. Geophys. Res.*, **110**, D13201, https://doi.org/10.1029/2004JD005501.

——, and J. Talamantes, 2006: Climate controls on valley fever incidence in Kern County, California. *Int. J. Biometeor.*, **50**, 174–182, https://doi.org/10.1007/s00484-005-0007-6.

——, H. S. Bian, and D. Newman, 2003: Mineral Dust Entrainment and Deposition (DEAD) model: Description and 1990s dust climatology. *J. Geophys. Res.*, **108**, 4416, https://doi.org/10.1029/2002JD002775.

Zhang, C. D., 2005: Madden–Julian oscillation. *Rev. Geophys.*, **43**, RG2003, https://doi.org/10.1029/2004RG000158.

Zhang, R. N., C. H. Sun, J. S. Zhu, R. H. Zhang, and W. J. Li, 2020: Increased European heat waves in recent decades in response to shrinking Arctic sea ice and Eurasian snow cover. *NPJ Climate Atmos. Sci.*, **3**, 7, https://doi.org/10.1038/s41612-020-0110-8.

Zhang, Y., Q. Z. Li, Y. Ge, X. Du, and H. Y. Wang, 2022: Growing prevalence of heat over cold extremes with overall milder extremes and multiple successive events. *Commun. Earth Environ.*, **3**, 73, https://doi.org/10.1038/s43247-022-00404-x.

Zhao, C., X. Liu, and L. R. Leung, 2012: Impact of the desert dust on the summer monsoon system over southwestern North America. *Atmos. Chem. Phys.*, **12**, 3717–3731, https://doi.org/10.5194/acp-12-3717-2012.

Brought to you by NOAA Central Library | Unauthenticated | Downloaded 07/19/23 05:08 PM UTC